Master's thesis
Master's programme in atmospheric sciences
Meteorology

Characterizing signatures of shipping emissions with satellite measurements of nitrogen dioxide

Elli Suhonen

August 6, 2021

Supervisor(s): Dr. Anu-Maija Sundström,
Assoc. Prof. Leena Järvi

Examiner(s): Assoc. Prof. Leena Järvi

University of Helsinki
Faculty of Science
PL 64 (Gustaf Hällströmin katu 2a)
00014 Helsingin yliopisto

HELSINGIN YLIOPISTO — HELSINGFORS UNIVERSITET — UNIVERSITY OF HELSINKI

Tiedekunta — Fakultet — Faculty	Koulutusohjelma — Utbildningsprogram — Degree programme
Faculty of Science	Master's programme in atmospheric sciences Meteorology

Tekijä — Författare — Author

Elli Suhonen

Työn nimi — Arbetets titel — Title

Characterizing signatures of shipping emissions with satellite measurements of nitrogen dioxide

Työn laji — Arbetets art — Level	Aika — Datum — Month and year	Sivumäärä — Sidantal — Number of pages
Master's thesis	August 6, 2021	50

Tiivistelmä — Referat — Abstract

International shipping is globally a major source of atmospheric nitrogen oxides (NO_x). It has been widely recognized that these emissions have negative effects on maritime air quality and human health. For a long time, shipping was the least regulated NO_x emission source, but now first regulations for ship exhaust NO_x emissions started as of January 2021. Shipping emissions must be monitored so the obedience of these regulations can be followed. Different measurement techniques are developed to address the problems related to shipping emission monitoring.

The purpose of this thesis is to demonstrate how tropospheric nitrogen dioxide (NO_2) concentration measurements by TROPOspheric Monitoring Instrument (TROPOMI) onboard Copernicus Sentinel 5 Precursor (S5P) satellite can be used to characterize signatures of shipping emissions. The capability of TROPOMI to detect busy shipping lanes and port areas was first tested with a large study area of the whole Eastern Mediterranean Sea. Analysis was supported with shipping emission data inventory from the Ship Traffic Assessment Model (STEAM). Results showed elevated NO_2 concentrations close to major port areas, especially if the dominant wind direction on the water area was from the continent. These elevated concentrations were most likely a result of both transported urban emissions and shipping emissions. STEAM and TROPOMI grid cell comparison was done over the busiest shipping lane area over the open sea, and the results showed that if the monthly summed shipping emission amount was either small or very large, the signal of shipping emissions was affected by background concentrations. More detailed shipping emission study was done at port Piraeus and the surrounding sea area. There, satellite measurement analysis was done by selecting three smaller study areas for comparison, one over the city of Athens, the second one close to the port Piraeus and the third one over the open sea. Relation between the satellite observations of NO_2 and modelled shipping emissions of NO_x was obtained in the study area that was over the open sea, the center of the area being 35 km from the coast. The signal of shipping emissions was not detected close to the port, most likely because of the influence of other emission sources. Lastly, spring and summer 2020 were analysed separately in more detail, as they were included in the overall study period of this thesis but the air pollution patterns at that time were affected by the extraordinary COVID-19 pandemic restrictions. The results showed unusually small average NO_2 concentrations over the city of Athens during spring 2020. Meteorological observations from that time period did not show anything that could fully explain the decrease. Observations over the sea close to Piraeus showed no clear difference between 2019 and 2020 average concentrations, so the pandemic possibly had only a minor impact on the shipping emissions in the port area.

Avainsanat — Nyckelord — Keywords

Säilytyspaikka — Förvaringsställe — Where deposited

Muita tietoja — Övriga uppgifter — Additional information

Acknowledgements

This thesis contributes to two EU funded projects: H2020 EMERGE and SCIPPER. EMERGE is coordinated by Finnish Meteorological Institute, and funded under H2020-EU.3.4 with grant agreement no. 874990. SCIPPER is funded with European Union's Horizon 2020 research and innovation programme under grant agreement no. 814893.

I kindly thank my employer Finnish Meteorological Institute for giving me the chance to study this topic. Atmospheric remote sensing group is an inspiring environment to do research, thanks to my colleagues there. Endless thanks to my thesis supervisor Anu-Maija Sundström for guidance and encouragement during this thesis process. I am grateful to my thesis supervisor and examiner Leena Järvi for good comments and discussion. I want to thank Henrik Virta for helping me with the data and letting me use his codes, and Iolanda Ialongo for all the help and advice during my employment. I am also grateful to Elisa Majamäki for providing me the STEAM datasets I needed.

Lastly I wish to express my gratitude to my family, my partner Aapo and my friends, for always supporting me.

Contents

Abbreviations

AIS Automatic Identification System

AMF Air Mass Factor

CRF Cloud Radiance Fraction

DOAS Differential Optical Absorption Spectroscopy

ERA5 European Centre for Medium-Range Weather Forecasts (ECMWF) Reanalysis version 5

ESA European Space Agency

GOME Global Ozone Monitoring Experiment

IMO International Maritime Organization

NECA Nitrogen Emission Control Areas

NO_2 Nitrogen dioxide

NO_x Nitrogen oxides

OMI Ozone Monitoring Instrument

PM Particulate Matter

SCD Slant Column Density

SCIAMACHY SCanning Imaging Absorption spectroMeter for Atmospheric CartograpHY

SCR Selective Catalytic Reduction

SECA Sulphur Emission Control Areas

SO_2 Sulphur dioxide

SP5 Sentinel 5 Precursor

STEAM Ship Traffic Emission Assessment Model

SZA Solar Zenith Angle

TEU Twenty-foot Equivalent Unit

TROPOMI TROPOspheric Monitoring Instrument

VCD Vertical Column Density

1. Introduction

Shipping is the most cost-effective way to transport cargo internationally, and that is why it has a major role in global trade [1]. Shipping is often referred as the most environment friendly way of transport. Nevertheless, ships constantly produce harmful substances into maritime air [2]. Ships produce exhaust emissions like sulphur dioxide (SO_2), nitrogen oxides (NO_x) and particulate matter (PM), and these emissions have negative effects on air quality and contribute to Earth's climate forcing [3]. The emissions cause health risk to densely populated coastal areas, as many of the pollutants from shipping are toxic to humans in high concentrations [4]. Shipping emissions are projected to increase steadily as global transport demand is expected to be growing continuously [5]. Regardless, emissions from shipping have been the least regulated emission source for decades [6]. To make international shipping more sustainable way of transport and to mitigate the health risk, the annual emission levels must be reduced measurably. The International Maritime Organization (IMO) has implemented progressive regulations to decrease shipping emissions, in particularly over environmentally vulnerable ocean areas [7]. The emission control areas are referred as Nitrogen Emission Control Areas (NECA) for NO_x pollution from ships and Sulphur Emission Control Areas (SECA) for SO_2 pollution [8] [9]. In Europe, these vulnerable ocean areas include the Baltic Sea and the North Sea for now. Expected growth of world's trade while facing the emission control is a challenge. Shipping emission monitoring must be done, so the compliance of these regulations can be followed [10].

The objective of this thesis is to show how satellite measurements of nitrogen dioxide (NO_2) concentrations can be used to characterize signatures of shipping emissions. Monitoring shipping emission signatures is overall known to be a challenge, especially over vast sea areas were continuous emission monitoring with ground-based stations is limited [10]. Space-borne measurements can offer nearly daily global coverage with good spatial resolution also over open sea areas, meaning that satellites could potentially offer a way to monitor shipping emissions. Therefore, it is important to investigate what is the sensitivity of satellite measurements to detect the shipping emission signatures. In this thesis, average NO_2 concentrations were characterized by using satellite measurements of TROPOspheric Monitoring Instrument (TROPOMI). TROPOMI

was launched to space onboard Copernicus Sentinel 5 Precursor (SP5) satellite in October 2017 [11]. Compared to its predecessors that monitor NO_2, TROPOMI has the highest spatial resolution, originally 7 km $\times$ 3.5 km and 5.5 km $\times$ 3.5 km since August 2019. TROPOMI measurements have been proven to be capable of detecting smaller NO_2 emission sources and concentration variations than previous instruments [12].
The focus area of this thesis is the Eastern Mediterranean. The first part of the results analyses qualitatively the NO_2 concentration distribution over this whole area. Over vast sea, areas influenced by shipping emissions can be identified by elevated NO_2 concentrations, as there are no other major NO_2 emission sources. However, detecting shipping emission signatures becomes more complicated close to coast, because there the satellite instruments can measure contributions from other emission sources. That is why the second part of the results is a local study close to the city of Athens and port Piraeus. The local study was done by selecting three different areas for comparison. The first area was in the middle of the city of Athens, the second at port Piraeus and the third area was over the open sea. Seasonal variations of NO_2 were characterized for each area to investigate their differences. For the two study areas covering the sea, the influence of shipping emissions on the satellite measurements of NO_2 was tested by estimating the consistency between averaged TROPOMI satellite measurements of NO_2 and data inventories by Ship Traffic Emission Assessment Model (STEAM) [13]. Moreover, as spring 2020 was included in the overall study period of this thesis, a separate analysis focusing on NO_2 concentration variations during that time period was done, as COVID-19 pandemic related restrictions on traffic, travelling and business affected the typical air pollution patterns [14]. The effects of the pandemic were analysed separately for each study area, to address how the restrictions possibly affected different emission sources.
This thesis has the following structure. Chapter 2 explains the characteristics of atmospheric NO_2. The chemistry of tropospheric NO_2 is introduced, with separated sections explaining the sources and effects of NO_2 pollution, the current situation of shipping emissions of NO_x, and details on the COVID-19 pandemic in Greece and how it affected the air quality. Chapter 3 goes through explanation of the satellite measurement principles and an introduction of TROPOMI satellite instrument. Chapter 4 has sections describing the data used in this thesis and description of the used analysis methods, following with a section describing the research area. Chapter 5 reports the results of this thesis. First section presents analysis on shipping emission signatures in the Eastern Mediterranean, and the second section presents the analysis done in the city of Athens, port Piraeus and the shipping lane area. Chapter 6 finalizes this thesis with conclusions.

2. Atmospheric nitrogen oxides

2.1 Tropospheric chemistry

Dry air has two major chemical components, nitrogen (78%) and oxygen (21%) [15]. The rest consist of mainly argon (0.9%) and trace gas substances (0.1%). Trace gases include for example carbon dioxide, oxides of nitrogen, ozone and methane. For trace gases, the most relevant layer of the atmosphere is the troposphere, where the majority of atmospheric mass (85%) is [15]. The troposphere is the lowest layer of the atmosphere, with the height from 5 km (poles) to 15 km (Equator) [16]. It is further divided into boundary layer (BL) and free troposphere. From these two, the boundary layer is closer to the surface. There, surface processes like shear and buoyancy effects cause vertical mixing of the air. Tropospheric chemistry is dominated by highly reactive pure oxygen molecules, like dioxygen (O_2) and ozone (O_3) [17]. These two molecules have the ability to oxidize other chemical substances [18].
Nitrogen monoxide (NO) has one oxygen atom whereas nitrogen dioxide (NO_2) has two oxygen atoms. These two are the main nitrogen oxides in the atmosphere, and together they are referred as NO_x. Out of these two, the primary pollutant that is emitted directly from a source, for example a ship engine, is NO. The usual formation of atmospheric NO happens during combustion of fossil fuels. In high temperatures of engines, atmospheric oxygen reacts with nitrogen. Formation of NO in high pressure and temperature usually happens by either of the following reactions [15]:

$$N_2 + O \longrightarrow NO + N \tag{R2.1}$$

$$N + O_2 \longrightarrow NO + O \tag{R2.2}$$

Nitrogen is usually in the molecule form N_2 in the atmosphere, so in reaction R2.1, nitrogen is from the atmosphere. In reaction R2.2, the one nitrogen atom is from the fuel. After these reactions, NO is released into the atmosphere and it is quickly oxidised, forming NO_2 as a result. The chemical transformation of NO to NO_2 can happen for example with the following reactions [19] [20]:

$$NO + O_2 \longrightarrow 2\,NO_2 \tag{R2.3}$$

$$NO + O_3 \longrightarrow NO_2 + O_2 \tag{R2.4}$$

$$NO + HO_2 \longrightarrow NO_2 + OH \tag{R2.5}$$

In these reactions, NO_2 is formed when NO is oxidized with oxygen (R2.3), ozone (R2.4), or hydroxyl radical (R2.5). The time required for these reactions is some minutes [15]. As the reactions are so rapid, the amount of NO_2 and NO are usually considered collectively as NO_x in the atmosphere [21]. Tropospheric ozone has especially important role in the cycle between NO and NO_2. Ozone is formed by chemical reactions between NO_x and volatile organic compounds (VOCs) under UV radiation [18]. In direct sunlight, NO_2 breaks within minutes back into NO, and it is oxidized by O_3 [17] [21]. More NO_2 forms as a result. Then the cycle starts again, and more NO_2 and O_3 are produced into the troposphere. This cycle is called photochemical cycle of tropospheric ozone [15]. In the troposphere, ozone is considered as a greenhouse gas and it contributes to global climate warming [22].

Nitrogen oxide molecules have short lifetime in the atmosphere, and that is why the molecules do not travel up to high altitudes. Model calculations have estimated that NO_2 molecules emitted from ship engines have a mean lifetime of 1.9 - 6.0 hours [23]. Nitrogen oxides are usually removed from the atmosphere by wet deposition. When nitrogen oxides react with hydroxyl radical, nitric acid forms for example in clouds [15].

$$OH + NO_2 \longrightarrow HNO_3 \tag{R2.6}$$

Nitric acid, HNO_3, can mix with water. If HNO_3 mixes with raindrops in clouds, it will fall down as acid rain. Reaction R2.9 is the largest global NO_x sink, accounting for 60 % of the total sink [24]. In the wintertime, this NO_x sink is much smaller compared to summer, because the amount of hydroxyl radicals depend on the amount of ultraviolet (UV) radiation [15]. Moreover, this means that NO_x sink is also dependent on meteorological conditions, as both moisture and effective UV radiation is required for Reaction R2.6. Because of this, NO_x molecules stay longer in the atmosphere during winter months. That results in naturally higher concentrations of nitrogen oxides compared to summer. The other reason for elevated wintertime concentrations is that especially urban emissions are generally larger during winter. This is attributed to heavier use of power plants to heat homes in the wintertime [20].

2.2 Sources, effects and reduction actions

Nitrogen oxide sources can be divided into anthropogenic and natural origin. Anthropogenic sources produce the majority of global NO_x emissions, fossil fuel burning being by far the dominant source of NO_x [15]. That is why the highest NO_x concentrations can be measured for example near big cities. The largest natural sources of NO_x are biomass burning and lightning. In the tropics, biomass burning due agriculture and deforestation is a major source of NO_x [15].

The main NO_x sources in Europe in 2018 are presented in Figure 2.1. Road transport takes the largest share, 39% of all emissions. Non-road transport, that includes international and national shipping, takes a 8% share. In addition to fossil fuel burning engines, other important anthropogenic sources of NO_x are energy production and manufacturing, like power plants and metal smelters. These both take 15% from the total emissions, as does agriculture. The shares of road transport and energy supply have decreased during 2010-2018 due effective emission restrictions [25] [26].

Atmospheric nitrogen oxides have negative effects on human health [4] [27]. Air pollution as a whole is the single largest environmental health risk in Europe, and nitrogen oxides are among the most toxic air pollutants. Usual health effects of atmospheric NO_x exposure are lung problems, infections or asthma, and long term exposure can even affect premature mortality [25]. As atmospheric nitrogen oxides also have a part in the formation of acid rain, they can also be harmful for the environment. Acid rain can ruin the quality of soil, as acidity of rain removes soil nutrients and minerals [21]. Also, quality of water can be ruined by acid rain, and in coastal waters it can cause a decline in fish and shellfish populations [28]. With air pollution regulations, prevalence of acid rain has successfully been reduced in Europe and Northern America. However, it remains a problem in many developing countries [17].

In addition to these local effects, nitrogen oxides also have a minor role in global climate change. Nitrogen oxides are called indirect greenhouse gases, so they do not directly affect greenhouse effect, but they can act as precursors for actual greenhouse gases like tropospheric ozone or particulate matter [22].

Because of all these negative effects nitrogen oxide emissions have on people, environment and climate, actions for air pollution reduction have been taken in the form of legal guidelines [21]. In Europe, the main legal guidelines are defined by European Environment Agency (EEA) [25]. Pollution controls mainly considers road-transport, power plants and factories. Shown by both model calculations and measurements, these controls have shown to be effective in Europe. Concentrations of almost all air pollutants have decreased throughout most of Europe since 1990 [29]. In 2018, NO_x emissions in Europe were 56% smaller than in 1990.

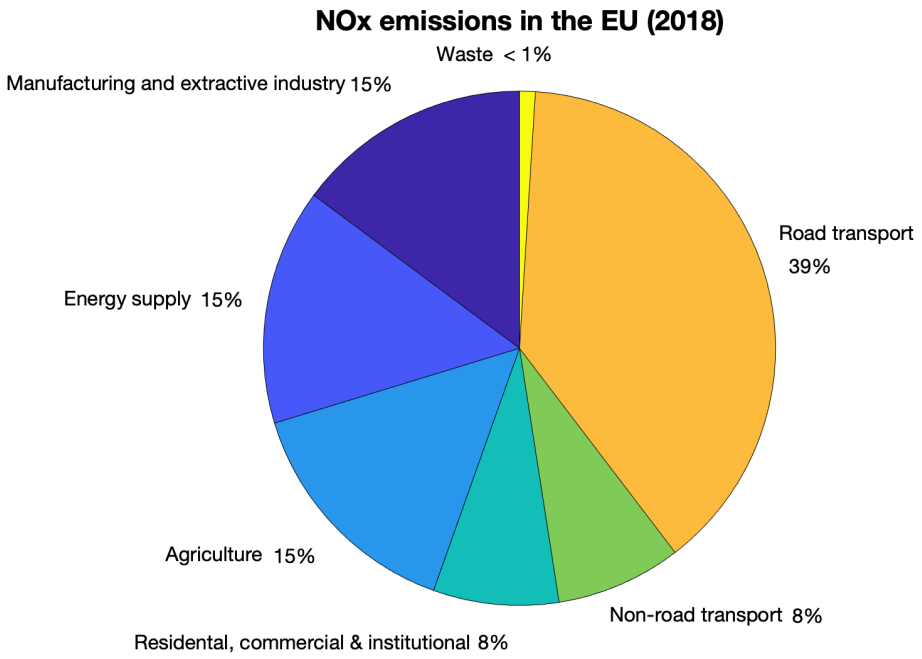

Figure 2.1: Main NO_x emission sources in EU in 2018. Data Source: Air quality in Europe - 2020 report: Sources and emissions of air pollutants [25].

Decline in emissions has directly affected the effects on human health. European Environment Agency estimated in their Air quality in Europe- report (2020) that NO_2 had impacted around 55 000 premature deaths in Europe (including 41 countries) in 2018. In 2009 the estimated impact was 120 000 premature deaths, so the impact had halved in almost a decade [25].

2.3 Emissions from shipping

International Maritime Organization (IMO), United Nations agency that authorizes security and environmental issues of international shipping, monitors that shipping companies do not compromise in maritime safety or pollution prevention protocols [30]. IMO estimates that more than 80% of the world's trade is carried by sea traffic. The estimated amounts of annual emissions from ships are 1.2 - 1.6 million metric tons (Tg) of particulate matter, 4.7-6.5 Tg of sulphur oxides and 5-6.9 Tg of nitrogen oxides [3] [27]. These emissions have a large impact on the chemistry of the marine boundary layer. Emissions from ships are mainly clustered along major ship routes in open seas or close to populated coastlines. Steady growth of shipping emissions is expected annually, as transportation capacity demands are growing.
In the near future SO_2 and NO_x emissions from national shipping can take a major

part of total national emissions of European countries, as other major emission sources have been restricted for a longer time [25]. European Union and IMO have stated progressive regulations on international and national shipping that will affect emissions of different relevant atmospheric gases. As of January 1st 2018, companies had to monitor each of their ships' carbon dioxide (CO_2) emissions and fuel consumption. Next, from 1st January 2020, ships were required to reduce SO_2 emissions by more than 80%. In Sulphur Emission Control Areas (SECA) all ships must use fuel with smaller sulphur content [9]. And lastly, as of 1st January 2021, all ships passing through Nitrogen Emission Control Areas (NECA) must use defined mandatory engine standards or equivalent NO_x emission reduction technologies to respect the stricter NO_x emission levels [8]. SECA and NECA, defined in the Convention for the Prevention of Pollution from Ships (MARPOL) protocol [7], do not consider all the sea areas in the world, but only the ones that have especially vulnerable marine environment. SECA and NECA include the Baltic Sea, North Sea, Caribbean and coastal waters of North America. Although these control areas do not include yet the Mediterranean Sea, which is the research area of this thesis, these restrictions put pressure on shipping companies to reduce their emissions overall.
The NO_x emission standards can be achieved by using additional technology in vessels, for example Selective Catalytic Reduction (SCR) devices [10]. Ideally used, SCR technology could cut NO_x shipping emissions by 90% [31]. However, SCR devices are not cheap. In addition, fuel that is low in sulphur content is considerably more expensive than fuel with high sulphur content. It cannot be taken as granted that all vessels are willing to follow the new regulations. Shipping emission monitoring has become more important as the obedience of the regulations must be followed, especially over vast sea areas. Restriction control is easier to execute close to ports, as open sea areas are far away from ground-based measurement stations.

2.4 Impact of COVID-19 pandemic on nitrogen oxide emissions

The global outbreak of SARS-CoV-2, also known as COVID-19 or coronavirus, was declared as Public Health Emergency of International Concern (PHEIC) by the World Health Organization (WHO) in January 2020 [32]. In March 2020 WHO declared the virus outbreak as a pandemic, Europe being the main area where the virus was spreading. As effective vaccinations were not available in spring 2020, many countries around the globe had to make public health actions to reduce spreading of the virus. These actions were referred as "lockdowns". The actions were mainly quarantine orders, restrictions to travelling and temporal closing of businesses and public spaces [14].
Satellite measurements detected unusual declines in average NO_2 concentrations over

cities in China, Europe, South Korea, and the United Sates after the outbreak of COVID-19 virus and the start of lockdown actions in spring 2020 [14]. As year 2020 is included in the study period of the satellite observation analysis of this thesis, the effects COVID-19 pandemic restrictions had on air pollution have to be acknowledged as a separate topic. As this thesis has the focus on the city of Athens and Piraeus port in Greece, the pandemic situation in Greece is considered here. Soon after first cases of COVID-19 virus in Greece were reported in February 2020 [33], General Secretariat for Civil Protection of Greece made orders of restrictions. During the beginning of March, schools were closed, followed by closing of museums, restaurants, malls, and other public places [34]. On 23rd March 2020 Greece's government ordered restrictions to all non-essential transport and movement. Industrial activities continued normally. Businesses and schools could be opened again starting 11th May 2020. Recent paper estimated that in March and April 2020, NO_2 concentrations in six largest Greek metropolitan areas reduced 3-26 % compared to emission levels of the previous year [35]. It was concluded that overall in Greek cities, the reduction of NO_2 in March-April 2020 compared to previous year was approximately 10 %.

The pandemic restrictions affecting the activities on Piraeus port are also considered here, because Piraeus is one of the focus locations of this thesis. Annual report by Piraeus port authority described that port passenger activity in Piraeus was affected by the COVID-19 pandemic restrictions [36]. Total passenger traffic experienced a 98.5% decrease between 2019 and 2020. Container volume of Piraeus port in 2020 was 5.43 million Twenty-foot Equivalent Unit (TEU), an unit referring to container terminal's capacity for cargo [1]. In 2018, volume was 4.91 million TEU [37], and in 2019, it was 5.65 milloin TEU [38]. In normal conditions the container volume was expected to increase in 2020 but instead it decreased. This is due to slowdown in economy. Nevertheless, the container terminal has been fully operational during the whole virus outbreak [36].

3. Satellite measurements of nitrogen dioxide

Nowadays satellite measurements are widely used to analyse atmospheric composition. One advantage of satellite observations is that they can be obtained over areas where ground-based measurement network is sparse or doesn't exist at all. Satellite measurement methods have developed rapidly during past years, and now daily NO_2 satellite measurements can be obtained with a pixel size of few kilometres.

3.1 Basic principles of satellite remote sensing of trace gases

Passive satellite instruments measure the backscattered solar radiation coming from the Earth. This solar radiation, that has travelled through Earth's atmosphere, has interacted with different atmospheric gas molecules. These interactions include scattering and absorption, where scattering changes the direction of light and absorption changes the form of radiation energy to something else, like heat. Absorbing substances in the atmosphere include aerosols like soot, or molecules like ozone, nitrogen dioxide and water vapour. Different gases and molecules in the atmosphere absorb radiation at different, specific wavelengths, and by that leave their own specific mark to the radiation. That mark can be identified from the radiation measured by a satellite instrument, and that information can be used to obtain the concentration of this gas from the measured intensity. Satellite measurement wavelengths are chosen based on the absorption wavelength of the substance that is supposed to be measured [17].
The physical background of the satellite trace gas retrievals is based on obtaining the original intensity of light and then the new intensity after it has travelled through atmosphere. Comparing these intensities reveals how the radiation has interacted with substances in the atmosphere. The calculation starts with the definition of the intensity of radiation. Wavelength dependent intensity of light, I, also called radiance, can be calculated as [17]:

$$I(\lambda) = \frac{\Phi}{\Omega A_s}, \tag{3.1}$$

where λ is the wavelength of the radiation, Φ is the radiant flux, A_s is the radiating area, and Ω is solid angle. Unit of $I(\lambda)$ is $\mathrm{Ws^{-1}r^{-1}\ m^{-2}}$. In an absorbing medium like the atmosphere, radiance of light attenuates. Absorption and scattering cause extinction of I, $dI(\lambda)$, and it can be defined:

$$dI = \frac{d\Phi}{d\Omega A_s} = -I(\lambda)\sigma_a(\lambda)Nds, \tag{3.2}$$

where $\sigma(\lambda)$ is the absorption cross-section of the absorber (molecule), indicating the probability of an absorption, N is is the number of absorbing molecules and the infinitesimal thickness of an absorbing layer is ds. If the thickness of the absorbing layer is defined as L, integration over the whole layer can be written as:

$$dI = -I(\lambda)\sigma_a(\lambda)\int_0^L Nds. \tag{3.3}$$

After reorganizing, the intensity of the radiation after travelling through the absorbing layer can be written as:

$$ln(\frac{I_0(\lambda)}{I(\lambda}) = \sigma_a(\lambda)\int_0^L Nds, \tag{3.4}$$

$$I_L(\lambda) = I_0 e^{-\sigma_a(\lambda)LN}, \tag{3.5}$$

where I_L is the radiance that the satellite instrument measures, whereas I_0 is the initial radiance emitted from the Sun, also called the solar irradiance. Equation 3.5 is called the Beer-Lambert law [17]. Detector, like a satellite instrument, measures the radiance I_L and irradiance I_0. Cross-section σ is defined by laboratory measurements. Wavelength λ is optimised for each trace gas separately, based on their own absorption wavelength spectrum. For example for NO_2, the absorption spectrum is 250 nm - 650 nm with the absorption peak occurring at 403 nm [39]. Naturally, the measurement wavelengths are usually chosen to be close to the absorption peak wavelength. When these parameters are known, the number of molecules, N, multiplied with the thickness of the atmospheric layer, L, can be calculated. This parameter, LN, can be also expressed as concentration, c. Its value tells how many molecules are in the defined atmospheric volume. Data is presented in unit of trace gas amount per atmospheric volume or area, for example molecules $\mathrm{cm^{-2}}$.

Basic physics of satellite retrieval of trace gases can be explained with the Beer-Lambert law. However, in real atmosphere the propagation of radiation is a much more complex process. In reality, multiple absorption and scattering processes happen along the path of the light. In addition, thermal emission can effect the intensity. To determine an accurate estimation of the concentration of a particular trace gas, it would require

the quantification of all other factors that influence the intensity of light along its path. These processes have to be calculated with numerical methods. One of the most commonly used spectroscopic methods to measure trace gases in the real atmosphere is called the Differential Optical Absorption Spectroscopy (DOAS) [17]. The DOAS method is based on the Beer-Lambert law (Eq. 3.5), but it is expanded to consider the other factors that affect the light on its path. DOAS algorithm considers the absorption of various trace gases, atmospheric Rayleigh and Mie scattering, instrumental effects and turbulence. The result is a polynomial for calculating the column concentration of real atmosphere, that can be solved with numerical data assimilation model.
Radiance and irradiance spectra measured by some satellite instrument is processed by a DOAS algorithm and the result is the slant column density (SCD) of some molecule. The product is for a slant column, because nadir-viewing imagers measure light path that travels in a slant path from the surface. The slant column retrieval is presented in Figure 3.1. After the retrieval of a slant column trace gas concentration, chemistry transport model is then used for dividing the total column to the the stratospheric and tropospheric columns. The model detects the stratospheric column by data assimilation methods with information on stratospheric chemistry [11]. In this thesis, the tropospheric column is used.

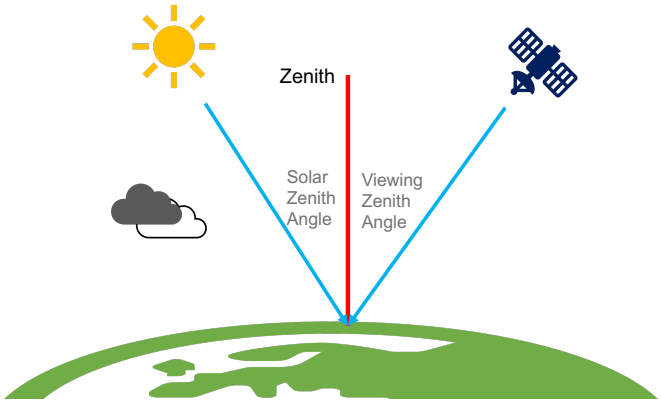

Figure 3.1: Illustration of the geometry of radiation satellite measurement. The blue lines are the optical light paths. These paths are slant columns, and the blue line reflected from the surface represents the column that is used for calculating slant column density (SCD). The red line illustrates the vertical column, which is relevant for calculating vertical column density (VCD).

SCD does not give information on the molecule concentration in the direct vertical air column above the ground pixel. The slant column geometry of satellite measurements is not constant around the globe, and therefore SCD measurements from different latitudes are not comparable. Moreover, if there were clouds present during the measurements, SCD contains only information on atmospheric column above clouds, because clouds effectively scatter away the radiation that would normally reach the surface. These are the reasons why SCD is not used for comprehensive satellite measurement analysis, but instead the slant column is converted into the concentration right above the ground pixel, called vertical column density (VCD). The vertical column geometry is presented in Fig. 3.1 as a red line. To calculate VCD, the viewing angle, the exact measurement location and the cloud coverage has to be taken into account. The slant column is converted into a vertical column by applying a tropospheric air mass factor [40] [11]:

$$V = \frac{S}{M}, \tag{3.6}$$

where V is the vertical column density, S is the slant column density and M is the air mass factor (AMF), which is obtained from a pre-calculated lookup table. The AMF depends on different factors that affect the measured slant column, for example viewing geometry, altitude, surface pressure, albedo and cloud pressure, height and fraction [11]. AMF includes correction if the measured light path was partly cloudy, and cases with full cloud cover are totally excluded, as trace gas concentrations are not obtained from these pixels. The AMF is always an approximation, and for it to be reliable, satellite solar zenith angle (SZA) <= 75 ° is required [17]. AMF has structural uncertainty of 42% over polluted regions and 31% over unpolluted regions [41]. Recent study found that TROPOMI NO_2 can possibly have the AMF attributed low bias in urban areas up to 20-40% [42].

3.2 TROPOspheric Monitoring Instrument

Uninterrupted series of NO_2 satellite measurements started in 1995 with European Space Agency (ESA) operated backscatter satellite instrument, Global Ozone Monitoring Experiment (GOME) [43]. With GOME measurements, the total vertical columns of NO_2 could be calculated with pixel size of 40 km × 320 km. The instrument following GOME was SCanning Imaging Absorption spectroMeter for Atmospheric CartograpHY (SCIAMACHY) onboard ESA's ENVISAT satellite, operating for ten years in 2002-2012 [44]. With improved resolution of 30 km × 60 km, SCIAMACHY started the modern space-borne research of atmospheric NO_2. The first studies on shipping emissions were done with both GOME and SCIAMACHY measurements, but the data had to be averaged for a long temporal period (several years) in order to detect ship

tracks [23] [45]. However, NASA operated Ozone Monitoring Instrument (OMI) was at its own time the biggest forerunner for measuring atmospheric trace gases [46]. Built by Finnish-Dutch cooperation, OMI was launched to space in 2004 aboard NASA's AURA spacecraft. The mission is ongoing, so it means that currently OMI has been measuring atmospheric trace gases for over 15 years. Spatial resolution of OMI is 13 km × 24 km, which was a great improvement compared to GOME and SCIAMACHY. OMI has been proven to be reliable in observing urban emissions as well as shipping emissions [47] [48] [49].

The successor of OMI is called TROPOspheric Monitoring Instrument (TROPOMI) [50] [11]. TROPOMI's measurement principles are based on the principles of OMI, but TROPOMI's largest improvements are finer measurement resolution and wider measurement wavelength spectrum. TROPOMI was jointly developed by The Royal Netherlands Meteorological Institute (KNMI) and ESA, and it was launched to space as a single payload of Sentinel 5 Precursor (SP5) as a part of European Union's Copernicus Programme on 13 October 2017.

TROPOMI's measurement principle is presented in Figure 3.2. TROPOMI has a 2600 km wide swath, which means the width of measurement area the satellite covers during every orbit. The original spatial resolution of TROPOMI was 7 km × 3.5 km at nadir, but it was improved to 5.5 km × 3.5 km in August 2019. Measurement period is about 1 second. This all means that every second TROPOMI measures 5.5 km × 2600 km area in the orbit, and the area is further divided into small pixels. With these measurement principles, TROPOMI achieves nearly global coverage in one day.

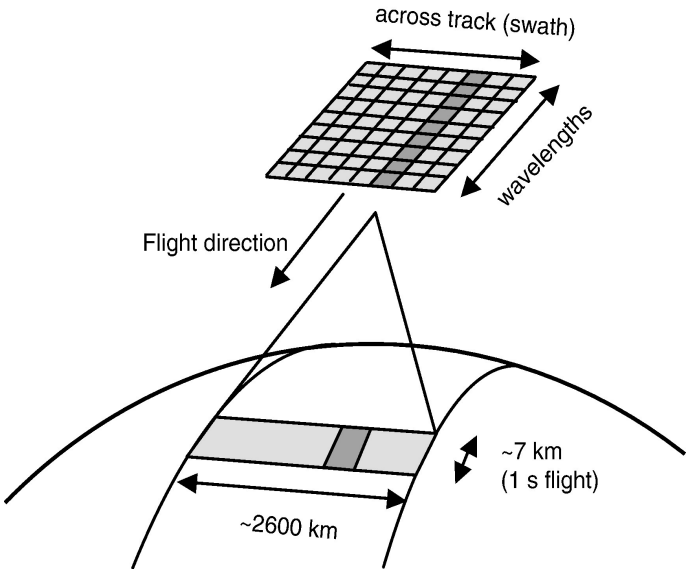

Figure 3.2: Illustration of TROPOMI satellite instrument measurement geometry. The swath width is 2600 km, and all pixels along that length are measured simultaneously. Size of one measurement pixel is 5.5 km × 3.5 km. TROPOMI's overpass is at 13:30 local time. Figure credit: Ref. [50].

SP5 is a low orbit satellite, flying at altitude of 824 km [50]. It has a polar and sun-synchronous orbit, meaning that it passes both poles during each orbit and has the same mean local overpass time at every given location on the Earth. SP5 daily overpass at ascending node is 13:30 local time. That means that daily TROPOMI measurements represent afternoon observations. One example orbit of tropospheric NO_2 observations by TROPOMI are presented in Figure 3.3. The figure shows how the orbit passes both poles. The effect of the quality flag filtering due clouds can be seen as white areas in the measurement swath.

TROPOMI measures different spectral bands, ultraviolet - visible (UV-VIS, wavelengths 270-495 nm), near-infrared (NIR, 675-775 nm) and short-wavelength infrared (SWIR, 2305-2385 nm) [50] [51]. With these measurement wavelengths, TROPOMI's measurements products include ozone, nitrogen dioxide, carbon monoxide, sulphur dioxide, methane, formaldehyde, aerosols and clouds. TROPOMI uses the same measurement wavelength range for NO_2 measurements as OMI, 405 nm - 465 nm [11]. Previous studies have demonstrated that TROPOMI is able to distinguish very local NO_2 sources and local concentration variations inside cities, factor areas, and busy transport areas like highways [12] [52]. Under favourable atmospheric conditions, TROPOMI measurements can be even used for detecting NO_2 plumes from individual ships [53].

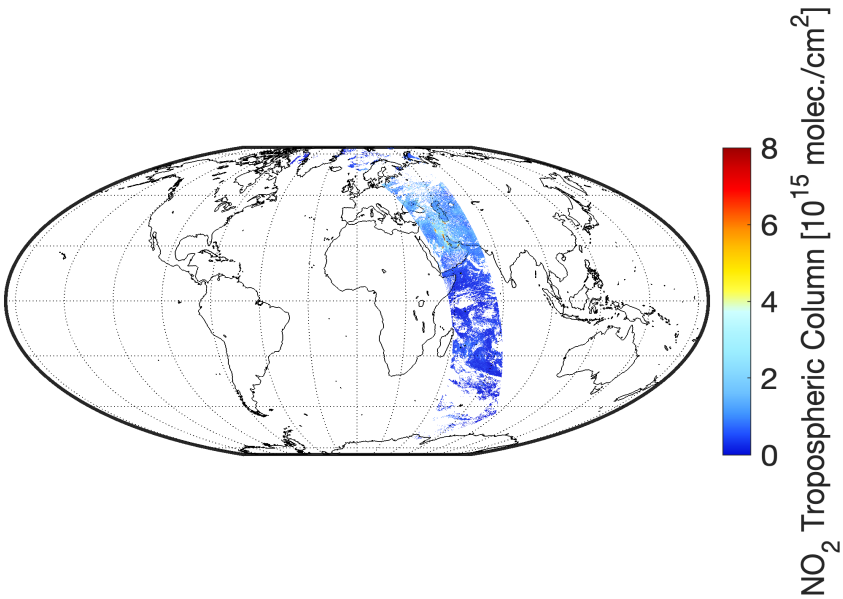

Figure 3.3: One example orbit of TROPOMI tropospheric NO_2 measurements from 23 August 2019. Measurements are filtered based on the effect of cloudiness and it can be seen as white areas among the measurements. Figure credit: Ref. [52].

4. Data and methods

4.1 Data

The main dataset of this thesis is TROPOMI Level 2 tropospheric NO_2 column concentration product, available for time period 30.04.2018 - 31.12.2020. This study period, defined by TROPOMI data availability, covers almost two years so comparisons between annual and seasonal averages can be done. The study period covers also the time period, starting from February 2020, when COVID-19 pandemic related lockdowns affected public behaviour. Average atmospheric NO_2 concentrations were impacted by these restrictive actions, and that is acknowledged in separate section in the results. Analysis on TROPOMI observations is supported by the European Centre for Medium-Range Weather Forecasts (ECMWF) reanalysis (ERA5) wind velocities and directions, along with shipping activity and exhaust emission data inventories by the Ship Traffic Emission Assessment Model (STEAM). Meteorological data from a ground-based station is used for analyzing the effects of COVID-19 pandemic on air quality in spring 2020. Basic information of these datasets are presented in Table 4.1.

Data name	**Data type**	**Units**	**Spatial resolution**	**Temporal coverage**
TROPOMI NO_2 Vertical Column Density (VCD)	Satellite measurements	molecules cm^{-2}	7.5 × 3.5 km 5.5 × 3.5 km (as of 08/2019)	30.04.2018 - 31.12.2020
TROPOMI Cloud Radiance Fraction (CRF)	Satellite measurements	Fraction	7.5 × 3.5 km 5.5 × 3.5 km (as of 08/2019)	30.04.2018 - 31.12.2020
ECMWF ERA5 wind velocity and direction	Reanalysis	ms^{-1}, °	0.25 × 0.25°	01.05.2018 - 31.12.2020
STEAM NO_x emissions	Model	kg	0.5 × 0.5 ° 1 × 1 km	05/2018 - 08/2018 05-08/2018- 2019
STEAM AIS messages	Model	Count	1 × 1 km	05-08/2018-2019
Air temperature	Ground-based	°C	Point	02-06/2019-2020
Wind velocity	Ground-based	ms^{-1}	Point	02-06/2019-2020

Table 4.1: Summary of the data used in this thesis.

4.1.1 TROPOMI tropospheric nitrogen dioxide

In this thesis, TROPOMI Level 2 NO_2 -product was used. Level 2-data consists of daily orbits of satellite observations. TROPOMI NO_2 Level 2-files in netdcf-format were downloaded from NASA GES Disc service. The main parameters are the total, tropospheric and stratospheric vertical column densities of NO_2, in addition with quality flag information and geolocations. The tropospheric column VCD was the main product used in this thesis. Quality flag information was used for filtering the data. Every satellite pixel that has a NO_2 retrieval value, is assigned with a quality flag, f_{ca}. The quality flag defines the quality and usability of the measurement pixel, and it is based on different factors that can affect the satellite measurement quality. These factors are for example cloudiness, large solar zenith angle, scenes covered by snow or ice, or other problematic retrievals [11]. Quality flag automatically removes pixels with too large cloud radiance fraction (CRF) value. If the pixel has CRF value larger than 0.5, it is not qualified for use. Moreover, as explained in section 3.1, qualified AMF requires that SZA is smaller than 75°. So quality factor automatically filters also away all pixels with too large SZA value. Quality factor itself has some value between 0-1. Value 0 indicates that some error has occurred during the processing and the measurement cannot be used. Value 1 indicates a perfect retrieval with no errors. Pixels with quality flag smaller than 0.75 are recommended to be filtered away. All TROPOMI observations used in this thesis were filtered by this standard.

4.1.2 Wind data

Although NO_2 is a short-lived gas in the atmosphere, strong winds can transport NO_2 molecules from their original source [47] [54]. When TROPOMI NO_2 data is compared to some other geographically interpolated data like STEAM products, strong wind can affect the interpretation of the results. If the molecules are transported away from their source, the spatial distribution of NO_2 concentrations over the original source area can seem smaller than it is, and the analysis becomes more complicated. That is why the prevailing wind conditions must be considered in the analysis.
ERA5 is the fifth generation of ECMWF's (European Centre for Medium-Range Weather Forecasts) atmospheric reanalyses, covering the global climate parameters [55]. Reanalysis combines real observations with models and data-assimilation systems to produce accurate climatic data archives. Reanalysis data can be downloaded from Copernicus Climate Change Service (C3S) Climate Data Store. The data used in this thesis was downloaded with Climate Data Store Application Program Interface (CDS API) as netcdf-files. In ERA5 datasets, vertical structure of the atmosphere is resolved using 137 levels from the surface up to the height of 80 kilometres. The levels can

be defined as pressure levels. For this thesis, mean values of U-component of wind, meaning the eastward wind, and V-component of wind, meaning the northward wind, on pressure levels 1000 hPa, 950 hPa and 900 hPa were downloaded. Pixel size of downloaded reanalysis data is $0.25° \times 0.25°$. The temporal resolution is 1 hour.

4.1.3 Ship Traffic Emission Assessment Model

In this thesis, an emission inventory is used to help detecting shipping emission signatures. The inventory used in this thesis is from the Ship Traffic Emission Assessment Model (STEAM). STEAM makes numerical estimates of trace gas emissions from ship traffic in European sea areas [13]. Modelled pollutants emitted by ships, given as a function of time and location, include nitrogen and sulphur oxides, carbon dioxide, particulate matter and carbon monoxide. STEAM has been proven to be reliable in high-resolution studies on shipping [56].

STEAM combines real-time shipping activity, air observation data, information on the pollutant streams in air and water, and reduction techniques for air and water pollution. STEAM uses Automatic Identification System (AIS), a ship identification and navigation system that is used by ships [57], to identify global shipping activity [58]. AIS produces datasets that consist of signals sent by ships. The signals include the unique identification of the vessel, its position, course and speed. These signals are referred as AIS messages. AIS messages must be sent with few seconds intervals by all international travelling ships weighting 300 gross tonnage and upwards, domestic cargo ships weighting 500 gross tonnage and upwards, and all passenger ships [57] [59]. STEAM can produce a geolocated grid of all AIS messages, so number of ships in certain areas can be calculated and the types of ships identified. After the ship types are identified, ship specific emission estimates can be done based on what kind of engines the ships should have. For each ship, the type of engine is available within AIS messages, and if it is not included in the message, the engine is assumed to be a medium speed diesel engine. Engine emission baselines are defined by IMO [7]. When the estimated amount of exhaust emissions are defined for each ship in the area, the total amount of emissions is calculated with specified STEAM resolution. The final result is a geographical grid, each STEAM pixel having the amount of emissions released into atmosphere within defined time range, for example during one hour.

In this thesis, two geographically gridded STEAM datasets are used. The first is gridded NO_x exhaust emissions from ships and the second is gridded AIS message count. The latter is used as an parameter representing shipping activity. For NO_x emission pixels, estimated bias is 10-20 %. STEAM NO_x emission data were available at two different resolutions. Large spatial scale that considers the total area of

Eastern Mediterranean Sea, had the spatial resolution of 110 × 110 km and temporal resolution of 1 month. Smaller study consider areas A2 and A3, that are presented in Fig. 4.2. Over these areas, STEAM data had pixel size 1 × 1 km, and the temporal resolution was 1 hour. Gridded AIS message data was available only for this smaller study area. The gridded emission datasets like the ones used in this thesis are available as netcdf-files upon request from the developers of STEAM [59].

4.2 Analysis methods

4.2.1 Gridding satellite observations

One Level 2- data file of TROPOMI contains measurements from one orbit of the satellite. Satellite measurement pixels on the Earth's surface do not necessarily have the equal size, and even the satellite orbits do not have exactly the same location every day [52]. That is why the measurement data must fitted into a regular spatial grid before it can be averaged for some time period. Observations must be also filtered so only satellite pixels with good quality are included in the final analysis. Data quality screening can in some cases filter out multiple pixels from measurements of one overpass. That can leave the daily NO_2 Level 2- data patchy, as it was seen in the example orbit in Figure 3.3. Therefore the data are averaged over a longer temporal time period. Spatial gridding and temporal averaging are done with gridding algorithms. The final satellite product that is filtered, gridded into a regular grid and averaged temporally, is called Level 3-data. Typical gridding algorithms use spatial interpolation, or present satellite observations as points or polygons [60]. Alternative algorithms use the original observations and average them into a new grid with specified resolution that is usually finer compared to the original resolution. This kind of methods are referred as "oversampling" [60]. In this thesis, two different resolutions were used for the oversampling. For maps with large spatial scale, the unified grid have a resolution of 3.5 × 3.5 km. Maps with smaller spatial scale have a resolution of 1 km × 1 km.
Oversampling starts by defining the required time range, for example one month. Then the research area is defined with coordinate limits. The algorithm creates an empty grid with the same latitude-longitude limits as the research area, but with new, specified resolution that is finer than the original measurement resolution. The algorithm goes through each Level 2 - TROPOMI files within the specified time range. First, the algorithm chooses only TROPOMI pixels that fall inside the desired latitude and longitude limits. TROPOMI pixels with low quality are filtered away. In addition, the average wind velocity over each TROPOMI pixel is calculated, and if the wind velocity was too strong in the area, the pixel is filtered away and not used. The definition of the surface wind velocity is explained in the next section. After filtering, the algo-

rithm compares the empty, fine resolution grid with the TROPOMI Level 2-file. The algorithm goes through all TROPOMI pixels and finds all the grid cells of the new, empty grid that have their centre within the area of some TROPOMI pixel. For those grid cells that are inside a TROPOMI pixel, the algorithm adds that corresponding TROPOMI pixel's NO_2 VCD value to the empty cells. The algorithm does this for each selected Level 2-files, and in the end, the new, fine resolution grid has vectors of added NO_2 values in the grid cells. After the algorithm has gone through every TROPOMI Level 2-file for the selected time period, the algorithm calculates an average of each grid cell, using the vector of the added values. So finally, the Level 3-file has a regular grid of averaged values with fine resolution. For this method to work the best way there has to be enough data available, so the selected time range should be long enough, at least few weeks [60].

4.2.2 Defining surface wind

As stated in section 2.1, after trace gases are emitted from their source they stay mainly in the tropospheric boundary layer. That is why only wind properties close to surface are relevant to know when analysing how molecules are transported by wind. In this thesis, average wind close to the surface is calculated with similar method as Ref. [47] used in their study. They calculated average wind velocity below 950 hPa pressure level. Also Ref. [54] used the same method and calculated average wind below 500 metres height. In this thesis, wind was averaged below 900 hPa pressure level. This method is not the most accurate for defining the exact average wind of the whole boundary layer, because variations in boundary layer height are not taken into account. This method can still provide useful results on surface wind direction and velocity when the study areas are large.

Average wind was calculated for each TROPOMI pixel area. This process started by reading ERA5 reanalysis files for the selected dates. The files contain wind grids where every cell had information on latitude, longitude, time, and u (northern) - and v (eastern) - wind components from pressure levels 1000, 950 and 900 hPa. For each grid cell, the final average u and v wind parameters were calculated by averaging over these three pressure levels. The average of these pressure levels represented the surface wind component. Wind data would be then linearly interpolated, so the wind parameters would work as interpolants in any point in time and space.

Mean wind over the area of every TROPOMI Level 2-file satellite pixel was then calculated by taking the central and corner coordinates of each TROPOMI pixel. Interpolated wind data was used to get wind parameters at these coordinates at the overpass time of TROPOMI. When the wind values at these locations and time was obtained,

the mean wind for the pixel was calculated. The information of wind conditions on every TROPOMI pixel was then used for filtering TROPOMI satellite pixels based on wind velocity or direction. The limit used for strong wind was 5 ms^{-1}. Wind directions were divided to four different sectors, northern (sector from north-west to north-east), eastern (from north-east to south-east), southern (from south-east to south-west) and western (from south-west to north-west). Wind from north has direction from 360°, from east 90°, from south 180° and from west 270° [61].

4.2.3 Comparing shipping emission and ship activity model data to satellite observations

The relations between TROPOMI and STEAM datasets were tested statistically in port Piraeus and the sea area south from the port. The STEAM data were studied on a monthly scale for both areas separately. The STEAM data consist on information of latitude, longitude, number of AIS messages and amount of NO_x emissions at 1 hour temporal scale. The data were filtered to contain results only from 10 - 12 UTC. This time period is the approximate S5P satellite overpass time over Greece. For each day, the NO_x emission amounts or AIS message amounts of the selected pixels were summed. The summation was done, because the data grids from one day contained usually many empty cells, so taking the total amount of emissions ensured that there is enough data to be compared with TROPOMI NO_2 concentrations. When the STEAM files of the specific month is considered, the total monthly sum of the area is calculated by adding all the daily sums. In the end, the final products for both areas were monthly total NO_x emission amount and total number of AIS messages sent in the area. These monthly sums were compared to monthly medians of TROPOMI NO_2 concentrations over these study areas.

It is to be noted, that the TROPOMI NO_2 measurement product used in this thesis has unit molecules per volume (molec. cm^{-2}) and STEAM gives the NO_x emission data as in unit mass (kg). These two variables do not represent the same quantity. Therefore, these two data products can not be compared by value. However, as the parameters are known to have some relation, it is expected that at some extent higher concentration should indicate higher amount of emissions. In this thesis, a good relation between satellite observations of TROPOMI and STEAM products indicate that there is some signature of shipping emissions found in the satellite observations.

Correlation between STEAM results and TROPOMI measurements was estimated with coefficient of determination, R^2. This coefficient is often used for comparing how model can predict variations in real observations.

R^2 is calculated with the following equation [62]:

$$R^2 = 1 - \frac{\sum_{i=1}^{n}(y_i - \hat{y})^2}{\sum_{i=1}^{n}(y_i - \bar{y})^2}, \tag{4.1}$$

where y in this case represents TROPOMI observations, n is the number of observations, $\hat{y}$ represents modelled values, in this case STEAM results, and $\bar{y}$ is the mean of TROPOMI monthly medians. Equation 5.1 gives a value between 0-1, and the number tells how well STEAM results can explain variations in TROPOMI observations. Value 1 indicates that the two datasets have a relation, value 0 indicates no relation. Coefficient of determination does not depend on unit, so even as STEAM and TROPOMI datasets do not have parameters that would have the same unit, the data products can be still statistically compared. To confirm the strength of the relation between the TROPOMI observations and STEAM results, p-value is used. P-value is often used in statistics to define the statistical significance between observations and model or test results [63]. P-value is calculated by taking a t-test, and the result ranges from 0 to 1. Values close to 0 indicate a significant correlation. The significance level is chosen to be the default value of 0.05. Usually p-values above this significance level are not considered to be statistically significant. It is to be acknowledged, that the p-value is not an absolute indicator of statistical significance, especially for complicated relationships. P-values can be negatively impacted by bias or small sample size. That is why the significance level is not absolute limit, but more a guideline [64].

4.3 Research area description

This thesis concentrates on satellite observations made in the area of Eastern Mediterranean. Shipping related, elevated NO_2 concentrations over open sea should be easy to detect because ship traffic on the Mediterranean sea is one of the most active in the Europe. For example in 2011, NO_x emissions from the ships in the Mediterranean Sea (1 229 000 t) were almost as high as those in the Baltic Sea (329 000 t) and the North Sea (649 000 t) combined [59]. Eastern Mediterranean is a good choice for satellite observation analysis in regards of satellite measurement quality. In low latitudes, like 0-30°N, solar radiation is available with low solar zenith angle for every season. In addition, compared to tropics, there are relatively few storms per year in subtropics. That also means that wind velocities are usually low so their effect on the NO_2 concentration distribution is minor. There is also a possibility for sun-glint in sub-tropical seas. Sun-glint is a phenomenon where the water surface acts like a mirror and the sunlight is reflected off the surface at the same angle as the satellite sensor views it. That strengthens the received signal and reduces the amount of noise in the satellite observations [53].

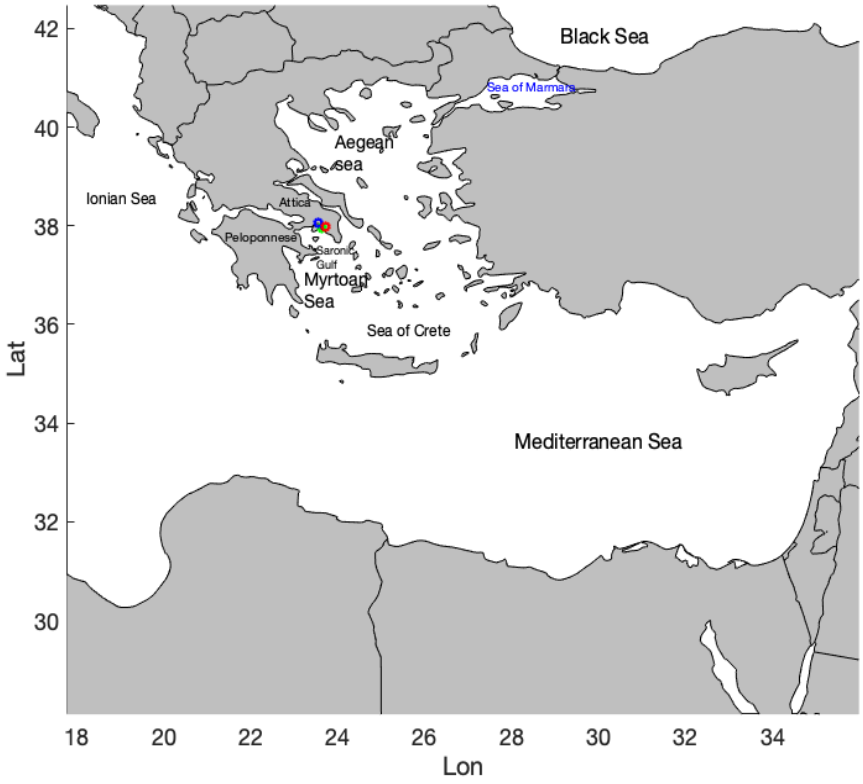

Figure 4.1: Map of the Eastern Mediterranean showing the overall study area of this thesis. Location of the city centre of Athens is marked with red circle, Piraeus port is marked with green circle and Eleusis airport is marked with dark blue circle.

Figure 4.1 shows an overall map of the Eastern Mediterranean. The city of Athens, Piraeus port and shipping lane over the sea were chosen as focus locations of satellite observation and shipping emission signature analysis. Piraeus port is the largest port in Eastern Mediterranean [65] [37]. Piraeus is situated in an advantageous geographic location, and it is part of the route that connects Europe with Asia. Athens and Piraeus suburbs are located in a narrow valley closed by mountains on the three sides and open to the sea on the south side. Moreover, Piraeus is one of most crowded port cities, hosting a large amount of people over a relatively small area [66]. Eleusis airport has a weather station close to Piraeus port and the city central of Athens. Locations of Piraeus port, city centre of Athens and Eleusis airport are marked in Fig. 4.1.
In Athens, three small research areas were selected for comparison. These three areas are estimated to be affected by different NO_x emission sources. The first area (A1) is in the city of Athens, the second area (A2) is the port Piraeus and the close by sea area, and the last area (A3) is over a open sea, the center of the area being approximately 35 kilometres away from the coast. A1 is expected to have emissions from urban sources,

like traffic and energy use. A2 is expected to be influenced with the emissions from the city, but it is also affected by emissions from the shipping traffic of Piraues port. Lastly, A3 is expected to be have more clear signal of shipping emissions, compared to the other two areas. The study areas with their exact geographical locations are presented in Figure 4.2, with the annual average (2019) tropospheric NO_2 concentrations measured by TROPOMI gridded into 1 km × 1 km grid. The total area shown in Fig. 4.2 has size of 77 km × 88 km.

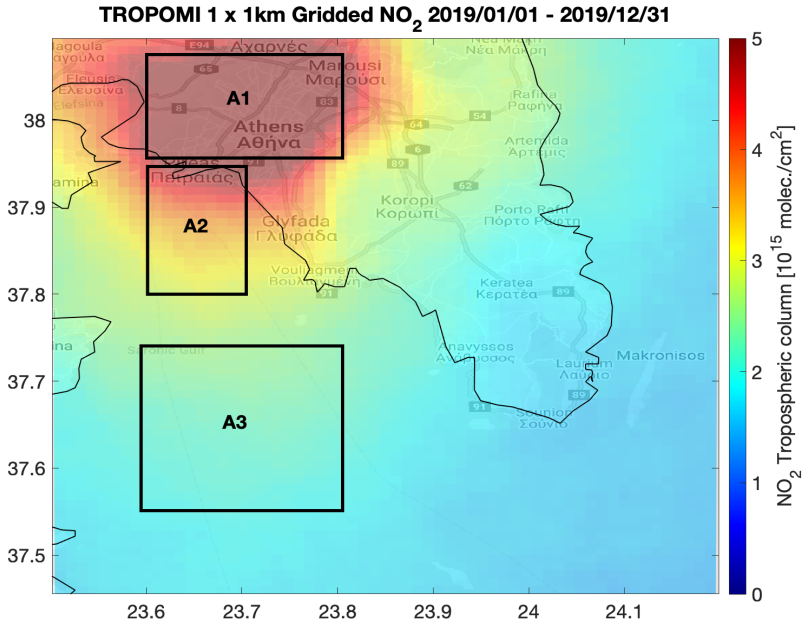

Figure 4.2: Annually averaged TROPOMI tropospheric NO_2 column concentration measurements of year 2019, gridded over the area that includes the city of Athens and the Saronic Gulf. Marked areas A1, A2 and A3 represent the three study areas used in this thesis.

5. Results

5.1 Overview of shipping emission signatures in the Eastern Mediterranean

Figure 5.1 shows a map of the Eastern Mediterranean with TROPOMI tropospheric NO_2 column concentrations gridded into 3.5 km × 3.5 km resolution and averaged over summer months (June, July and August) in 2018. Only measurements with weak wind conditions (wind velocity < 5 ms^{-1}) are included. After quality flag and wind filtering, the mean of each grid cell was calculated on average with 40 satellite observations. In this map, elevated tropospheric NO_2 concentrations reveal areas that have major NO_x sources, because the effect of transport by wind is filtered.

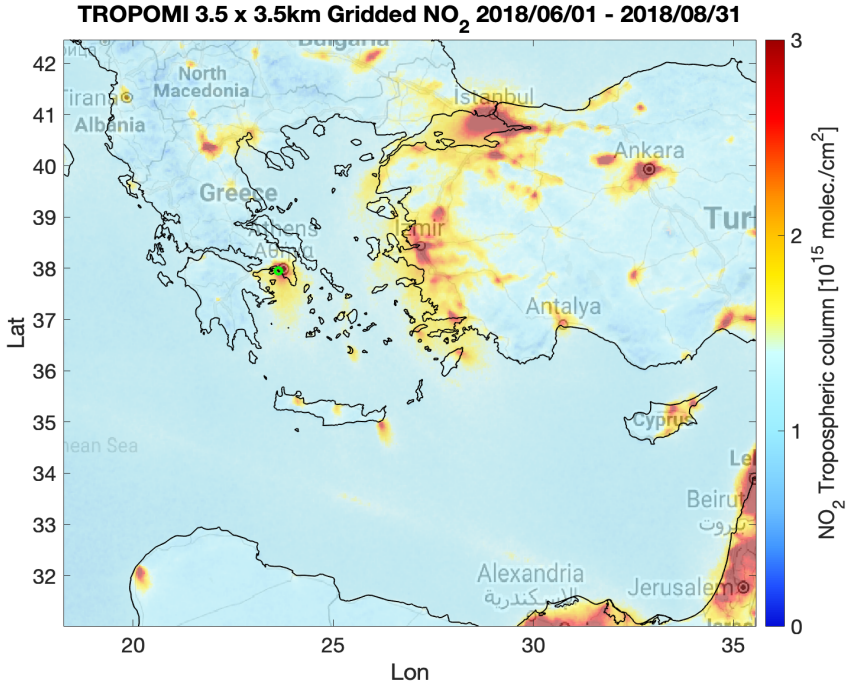

Figure 5.1: TROPOMI measurements of tropospheric NO_2 VCD, averaged over June-July-August (JJA) 2018 and gridded into a 3.5 km × 3.5 km grid over the Eastern Mediterranean. Location of Athens, which is the case study city of this thesis, is marked with a green circle. Coastlines are by Natural Earth (public domain at naturalearthdata.com). Geographical information is a Google maps product by Ref. [67].

The highest NO_2 concentrations can be observed over major coastal cities, as they are usually the most densely populated and have a lot of emissions from anthropogenic activities. Most populated cities like Istanbul, Alexandria and Athens stand out with elevated NO_2 concentrations on the map. Also sea areas close to Athens and Istanbul have higher NO_2 concentrations compared to the open sea. In these cases, as the effect of transport by wind is reduced, it is likely that at least some of the emissions originate from sources at the sea. Nearby islands south-east from Athens force cargo ships to take the straight route towards north when arriving to port Piraeus, and towards south when leaving the port. For that reason it could be assumed that shipping emissions accumulate over the Myrtoan Sea. The city of Istanbul has the same kind of situation, with the Sea of Marmara located west of the city. The narrow inland sea keeps the emissions from ships clustered over this small area, and urban emissions from the city are likely to be transported there as well. The sea of Marmara is a well-known sea area with major environmental problems due to the chemical pollution caused by shipping and urban emissions [68].

Figure 5.2 shows the STEAM NO_x emissions produced by ships, averaged over summer months of 2018 over the same study area as TROPOMI NO_2 column concentrations in Figure 5.1. This map reveals areas that are highly influenced with shipping emissions of NO_x. Comparing Figures 5.1 and 5.2 can qualitatively reveal where high tropospheric NO_2 concentrations coincide with large shipping emissions. The relative geographical distribution of the shipping emissions and elevated NO_2 concentrations seem to be fairly similar. For example, this comparison confirms that Istanbul and Athens are the two cities that have the most shipping emissions produced regularly within close distance from the city.

Fig. 5.2 shows pronounced amount of shipping NO_x emissions close to the start of the Suez canal in Egypt. That is not seen very clearly in Fig. 5.1, because the area with elevated NO_2 concentrations is not large close to the North African coast. There, elevated NO_2 concentrations are only covering the area very close to the start of the canal. One possible reason could be that the dominating wind direction is affecting the concentrations. Further investigation of ERA5 wind data showed that the dominant direction of the wind at the start of the Suez canal is towards the continent. Therefore, the shipping emissions are transported towards the land and also the effect of urban emissions over the sea is small. Instead in Athens and Istanbul, the mean wind is from the continent towards the sea. It means that there, the wind creates effective outflow from the city, and the urban emissions are transported over the sea. It might be that more strict wind filtering, for example with strong wind limit 3 ms^{-1}, would show better the elevated NO_2 concentrations by TROPOMI over the same areas where STEAM shows high amount of shipping emissions.

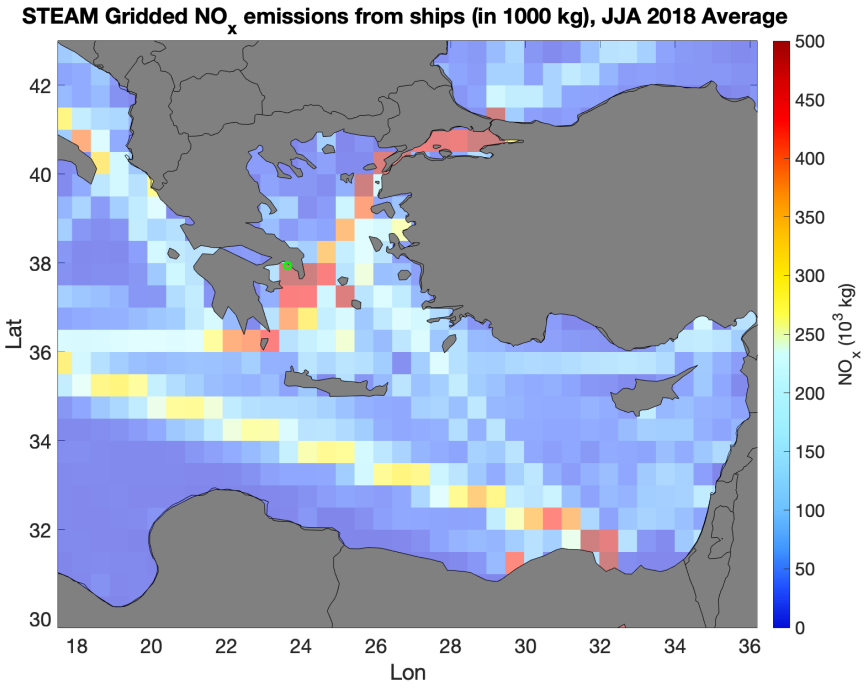

Figure 5.2: Gridded shipping NO_x emission data produced by STEAM. Data is averaged over June-July-August (JJA) 2018. Resolution of the gridded data is 0.5 ° × 0.5 °. Location of Athens, which is the case study city of this thesis, is marked with a green circle. Color scale is set so busiest shipping areas show as light blue, yellow or red. Country borderlines are plotted with borders-package of Climate Data Toolbox for MATLAB, where the data is compiled from 2013 US Census Bureau 500k and TM World Borders 0.3 datasets (thematicmapping.org) [69].

In Fig. 5.1, a line-shaped slightly elevated NO_2 concentrations over the sea area between the island of Crete and Northern Africa reveals a location of an active shipping lane. That shipping lane is known to be densely trafficked shipping lane of cargo ships [59]. It can also be seen as high amount of shipping emissions in Fig. 5.2 The TROPOMI map does not show any other ship tracks as clearly in this area. Adjusting the color scale for TROPOMI measurements in Fig. 5.1 could reveal these shipping lanes, but that would also enhance the background concentrations. This open sea area is chosen for more exact comparison of TROPOMI NO_2 observations and STEAM NO_x emissions. For this comparison, TROPOMI and STEAM are averaged over June, July and August 2018 and gridded into a same resolution, 0.55° × 0.55 ° within coordinates limits of 31.5-34.8 °N and 20-35 °E. As the datasets are gridded into the same resolution, at each location the averaged grid cell values of TROPOMI and STEAM can be compared. For TROPOMI observations this resolution is coarse, so the grid cells have averages of many TROPOMI observations in the area. This comparison of data grid cell values is shown in Figure 5.3. In this kind of analysis it should be also noted that there can be temporal gaps in the satellite observations due to clouds, whereas

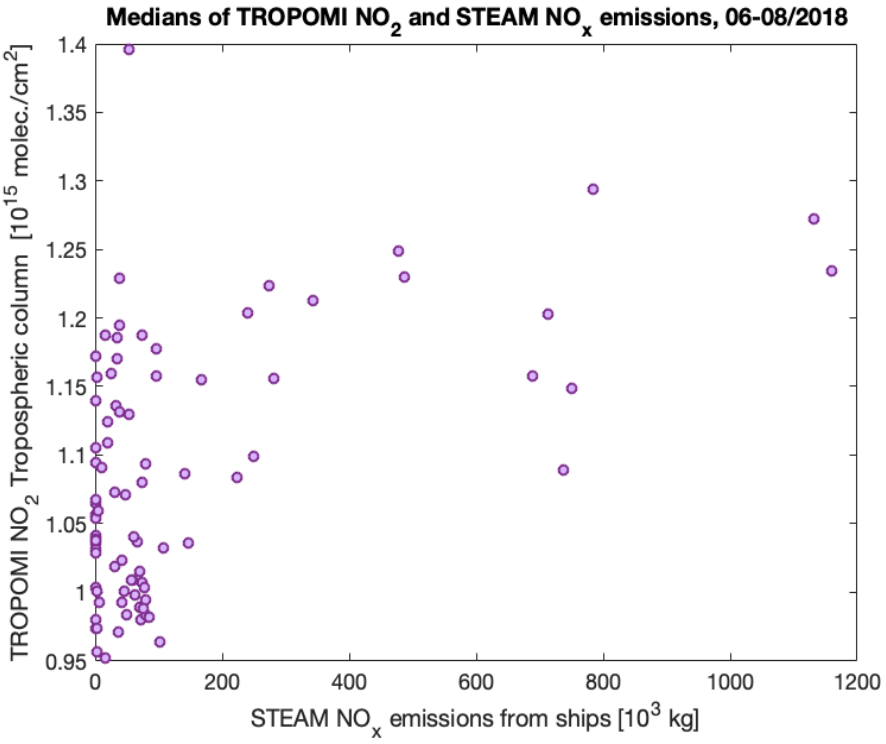

Figure 5.3: STEAM NO_x emission pixels averaged over the summer months (JJA), compared to summer months median of TROPOMI NO_2 satellite pixel values (resolution 0.55 × 0.55 °) . The two datasets show a statistically significant relationship ($R^2 = 0.26$, $p < 0.001$).

the model data is unaffected by this. Fig. 5.3 shows overall a statistically significant relation between the datasets, with $R^2 = 0.26$ and $p < 0.001$.

From Fig. 5.3 it can be seen that when the monthly STEAM NO_x emissions are approximately larger than 100 t, they seem to follow a linear trend and correspond to the average TROPOMI concentrations quite well. When the estimated shipping emission amount is smaller than that, the relation is not clear. When the small STEAM emission values correspond to the high NO_2 concentrations measured by TROPOMI, it could be that the satellite observations are from an area close to the coast where urban emissions influence the TROPOMI NO_2. On the other hand, the highest STEAM shipping NO_x emission amounts (> 1000 t) do not follow the linear trend that well either. The largest values of NO_x emissions were obtained from the area close to Suez canal. It was already qualitatively observed that over this sea area, that the STEAM model results shows pronounced amount of shipping emissions, but TROPOMI measurements do not show elevated concentrations at the expected magnitude. It highlights the previous indication that wind conditions might have an important role when analysing signatures of shipping emissions from satellite observations obtained close to the continent.

When the distribution of the TROPOMI NO_2 observations was investigated within

single grid cell, it was shown that the number of background-level NO_2 observations was high. There were also elevated NO_2, most probably related to shipping. When calculating the median over the whole pixel area, meaning the value one TROPOMI data point in Fig. 5.3, the contribution of these elevated concentrations is not seen because of the dominating background concentrations. So the signal from shipping tends to average out. That could explain why in Fig. 5.3 the large shipping emissions do not correspond to as highly elevated TROPOMI NO_2 as would have been expected.

5.2 Athens, Piraeus port and the shipping lane area

5.2.1 Seasonal cycle of nitrogen dioxide concentrations

Time series of monthly average TROPOMI NO_2 concentrations for study areas A1, A2 and A3 are presented in Figure 5.4. Monthly average concentrations show how emissions vary seasonally. The averages are calculated with TROPOMI Level 3- files that have monthly averaged NO_2 concentration grids. These averages are not filtered based on the wind velocity.

Area A1, that covers the city central of Athens, has the highest monthly mean tropospheric NO_2 concentrations. A1 also has the largest differences between the concentrations. The ratio of the lowest monthly mean to the highest monthly mean is 41%. The smaller the ratio, the larger the difference between the lowest and highest average concentration. That small ratio is in line with previous studies, that have concluded that urban emissions have typically different magnitudes seasonally [70]. In the summer, average concentrations of NO_2 are smaller, because the natural NO_2 sink is larger. In the winter, concentrations are larger because the lifetime of molecules in the atmosphere is longer, but also wintertime emissions are usually larger. In Athens, domestic heating takes share of 40% of the total emissions, so that has a large effect on wintertime emissions [71].

Over areas with anthropogenic NO_x sources, sudden changes in traffic or other human activities can affect the monthly average concentrations. Comparing the monthly averages of all the study areas, it seems that A2 and A3 have smoother seasonal variations in concentrations than A1. During the study period, there is at least three known major events that have affected monthly mean concentrations in A1. First case is from spring 2020, when COVID-19 caused decrease in many anthropogenic activities. The effect is seen the most in March 2020, when the monthly average concentration was clearly lower than usual. Then in July 2018, an extreme heat wave in Europe caused wildfire events in the Attica region [25]. Forest fires and warm weather with no rain were the reasons why the mean NO_2 concentration of July 2018 was larger than typical [25] [72]. Also April 2018 mean NO_2 concentration was larger than typical, most likely

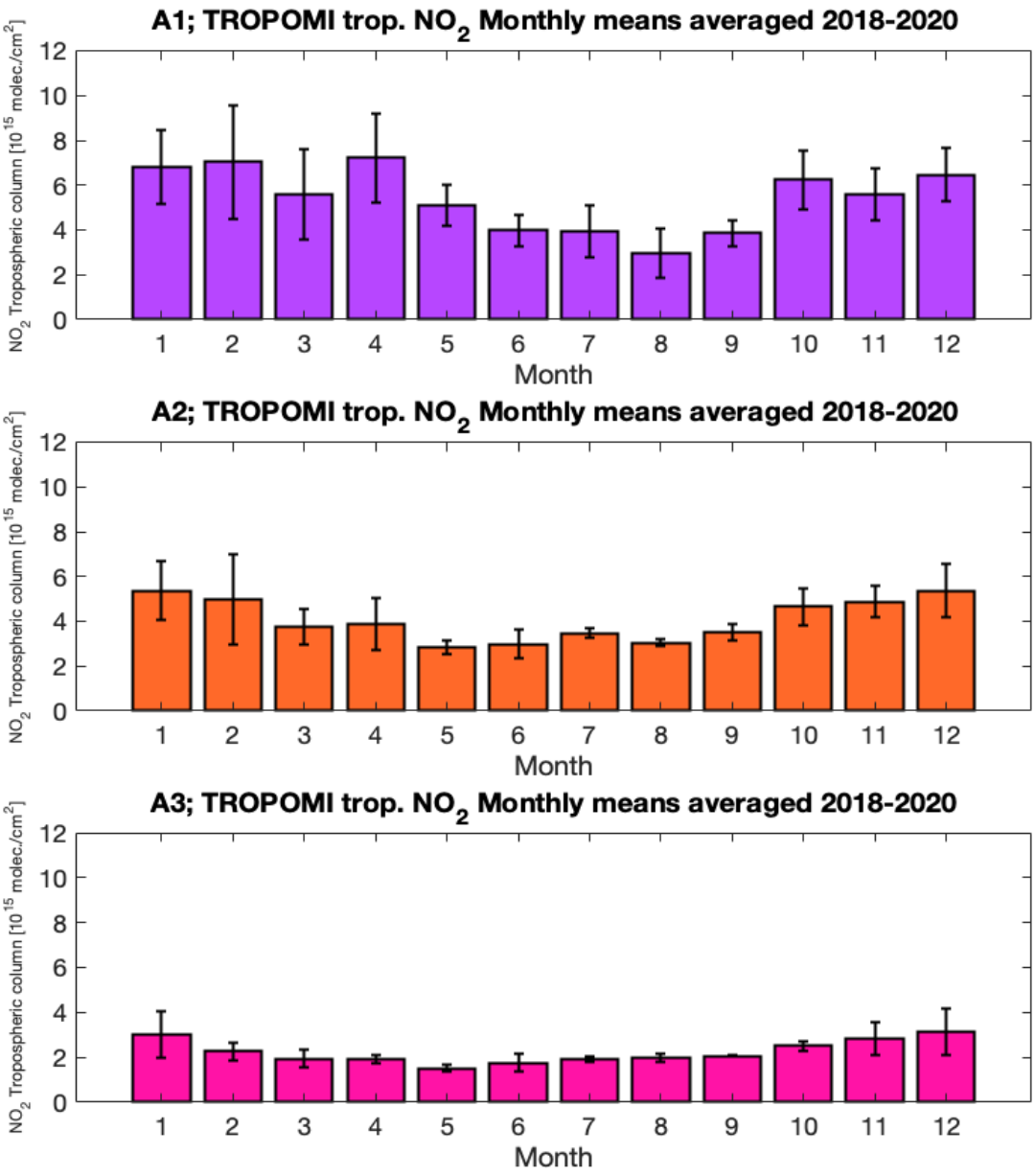

Figure 5.4: Monthly means of tropospheric nitrogen dioxide concentrations from areas A1, A2 and A3, defined in Figure 4.2. The means are calculated with gridded Level 3-data of TROPOMI monthly averages from 1st February 2018 to 31st December 2020. Marked errors show the standard deviation of the monthly averages.

because of a heat wave that occurred in Europe during that month.
Area A2 has lower monthly average NO_2 concentrations compared to A1, and also the seasonal cycle of NO_2 is more well-defined. The ratio between the lowest (May) and the highest (December) means is 53%. Large ratio means that the difference between the lowest mean and highest mean is small. During winter, the emissions from the city of Athens have the largest contribution to the NO_2 levels, as NO_2 molecules can travel farther away from their inland sources. That is most likely why December is having the highest average concentration. However, shipping activity minimizes during winter and maximizes during summer, because smaller vessels are active only during summer. Also cruise activity is more pronounced in summer. It means that during summer, when the contribution of urban emissions is smaller, the shipping emissions compensate and produce more emissions. This could explain why May has the lowest average concentration, along with natural seasonal variation of the NO_x sink. June, July and August could be influenced by emissions from the busy shipping traffic, so that is why they are not having the lowest mean.
Wind direction statistics for every season in area A2 are presented in Table 5.1. In Piraeus area, northern, western and eastern wind can transport air from the city to the sea. South is the only direction for wind to transport air from the sea to land. Spring and autumn are the seasons that most likely have wind also from the sea towards the continent, because temperature differences between land and sea can be large. That means that during spring and autumn the residents of the coastal areas are affected by shipping emissions the most.

Wind directions	**DJF**	**MAM**	**JJA**	**SON**
Northern (%)	73.2	62.1	89.9	74
Eastern (%)	0	4.2	0	0
Southern (%)	5.7	17.3	4.3	15
Western (%)	21.1	16.4	5.8	11

Table 5.1: Wind direction statistics on area A2 for every season. The seasons are marked with initials of the months of different seasons. Statistics are calculated with ECMWF ERA5 reanalysis dataset for dates 01.12.2019 - 31.11.2020. Only dates that have qualified TROPOMI measurements are chosen.

Northern winds seem to dominate during every season. That indicates that then urban emissions are regularly transported to the sea, creating good ventilation in the city of Athens. This was also speculated in section 5.1, as the NO_2 plume from the city of Athens seemed to spread southwards. The winter months are having the strongest winds on average and also the NO_x molecules stay longer in the atmosphere. Based on this, the monthly average NO_2 concentrations of winter months in areas A2 and A3

are influenced by urban emissions the most.

In area A3, monthly average NO_2 concentrations are lower compared to the other two areas. The seasonal cycle is still very similar to area A2, May having the lowest average concentration and December having the highest. The difference between the lowest monthly mean and the highest monthly mean is 52%, almost the same as in area A2. Area A3 is located south from area A2, and as northern winds dominate, emissions from the port are transported towards area A3. Areas A2 and A3 seem very similar, but area A2 is still estimated to be more influenced by urban emissions. The fact that area A3 has more well-defined seasonal cycle, monthly mean concentrations first decreasing and then increasing steadily, could indicate that the effect of urban emissions is smaller in area A3. This is useful information in shipping emission signature analysis, as it is expected that area A3 is far enough from the coast to represent different conditions compared to the port Piraeus area.

5.2.2 Signatures of shipping emissions in TROPOMI NO_2 observations

Figure 5.5 shows monthly medians of TROPOMI tropospheric NO_2 concentration measurements in area A3 are compared to monthly summed emissions of NO_x emissions modelled by STEAM.

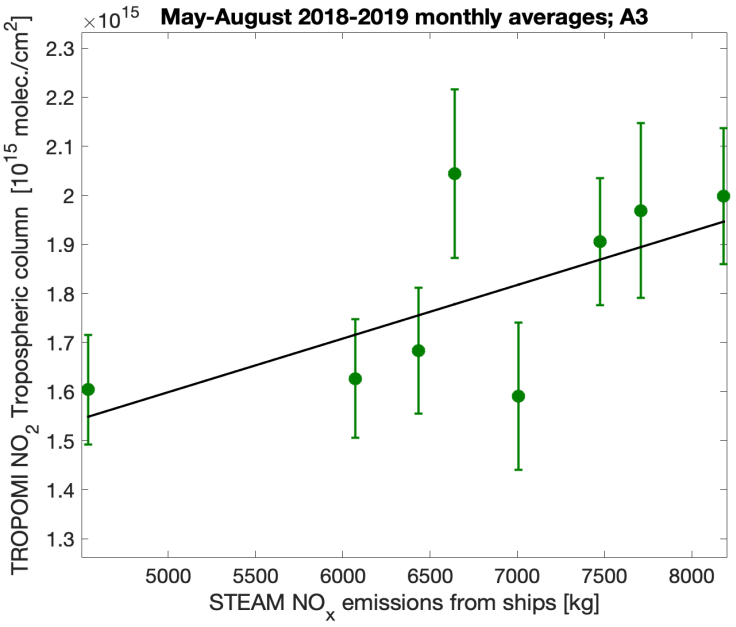

Figure 5.5: Monthly sum of STEAM NO_x emission amounts compared to monthly median of gridded TROPOMI NO_2 measurements in area A3. Both data had resolution 1 km × 1 km. Data points represent four months of two years, May - August of years 2018 and 2019. For comparison statistics were calculated $R^2 = 0.45$, $p = 0.07$.

Relation between these datasets would indicate that the satellite observations show a signal of shipping emissions. Only summer months are included, because then the ship activity is the greatest and the effect of urban emissions sources, that may affect the concentrations this close to the coast, are smallest as the natural NO_2 sink is effective. Fig. 5.5 shows that TROPOMI measurements of NO_2 and STEAM NO_x emissions are showing a positive linear trend. Coefficient of determination has value $R^2 = 0.45$ and p-value is $p = 0.071$. With the significance limit of $p < 0.05$, the result is slightly non-significant. However, the statistical comparison is affected by the small sample size of co-located observations. In this case, the significance limit (0.05) is not considered as an absolute limit defining the quality of results. Knowing that, the results indicate that a signal of shipping emissions can be seen in the satellite observations from A3. There was no correlation to be found between TROPOMI measurements of NO_2 column concentration and summed AIS message amount, as seen in Figure 5.6. The coefficient of determination R^2 of 0.001 and p-value of 0.9 indicate that there is no relation between these two datasets. This does not necessarily indicate that medians of TROPOMI NO_2 concentrations in this area are not influenced by ship traffic activity. The reason for the bad correlation could be that the AIS messages should be filtered in more specific way.

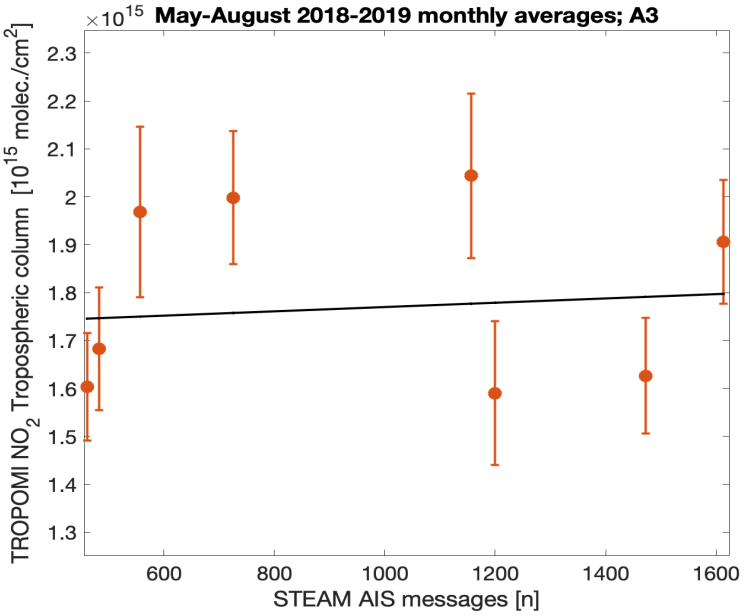

Figure 5.6: Monthly sum of STEAM gridded AIS messages compared to monthly median of gridded TROPOMI NO_2 measurements in area A3. Data points represent four months of two years, May - August of years 2018 and 2019. $R^2 = 0.001$, $p = 0.9$.

It could also be, that summed AIS messages are not suitable indicator for shipping activity for this kind of comparison, because the data consist of messages sent from all kinds of vessels. Emissions from multiple small ships are low and TROPOMI cannot detect the signatures of shipping emissions, even though the AIS data suggests that the shipping activity is high.
When this same analysis was applied to area A2, there was no correlation to be found with monthly summed STEAM NO_x emission data or summed AIS messages and TROPOMI NO_2. It suggests that area A2 is influenced too much with urban emissions, so analysing the shipping emission signatures is more complex. Modelling emissions close to port areas is overall quite difficult, because the ships might behave in unpredictable ways and the total amount of emissions is not easy to estimate.

5.2.3 Nitrogen dioxide concentrations in Athens during COVID-19 pandemic

As described in section 2.4, COVID-19 pandemic restrictions in Greece were relatively strict during spring 2020. There was a period when all non-essential movements were restricted. Recent studies have observed that in Athens, changes in public behaviour caused a decrease in the NO_2 concentrations. The study areas of A1, A2 and A3 are used again for analysing the effect the restrictions had possibly on different emission sources. The hypothesis is that urban emissions decreased more compared to shipping emissions. In practice it would mean that Central Athens (A1) had a more significant decrease in emissions, and the Piraeus port area (A2) and the open sea area (A3) did not have clear declines in concentrations.
Figure 5.7 shows map of Athens and Piraeus port with the difference of 2019 and 2020 spring (March, April, May) averages of TROPOMI tropospheric NO_2 column concentrations. Only measurements days with weak winds (wind velocity < 5 ms^{-1}) are included. Locations that have negative values on the map indicate that there, spring 2020 concentrations were lower compared to the corresponding period in 2019. It can be seen that the majority of the land areas have pixels with negative values. The difference is especially large over the central Athens and the northern parts of the city. On average for the whole area seen in the map, 2020 NO_2 concentrations were about 20% smaller than average concentrations of 2019. Negative values are seen also over Piraeus sub-urban and the port area. This is could be because at least in March, there were some restrictions on ships arriving to the port. For example, cruise ships were banned from docking at the port until everyone abroad was tested for COVID-19 virus [36]. Sea areas farther away from the coast are not showing a major difference between 2020 and 2019. The sea area west of port Piraeus shows that the spring 2020

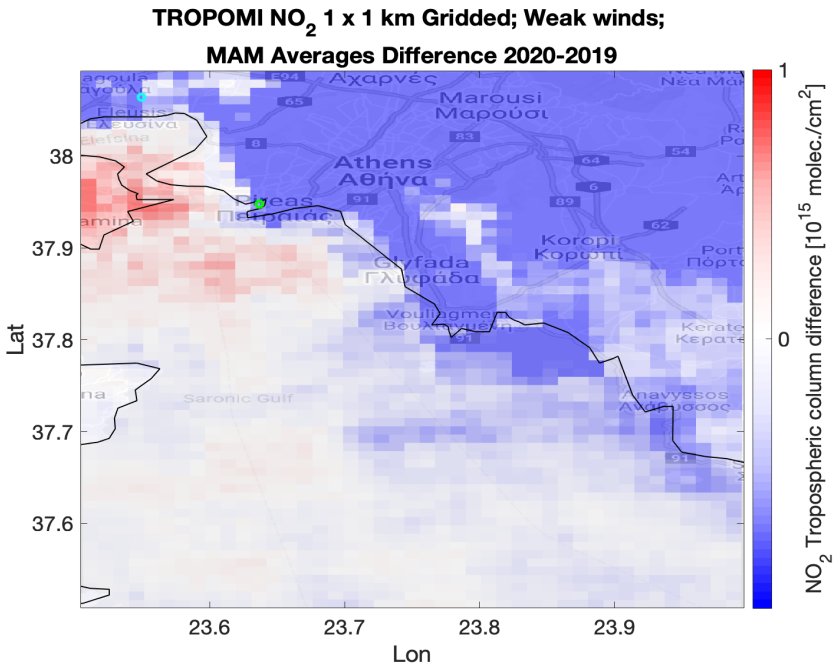

Figure 5.7: Difference between spring averages of 2020 and 2019 of TROPOMI tropospheric NO_2 column concentrations. Only days with weak wind are included (daily average wind velocity $< 5\text{ms}^{-1}$). Location of the Piraeus port is marked with green circle, and location of the Eleusis airport is marked with cyan circle.

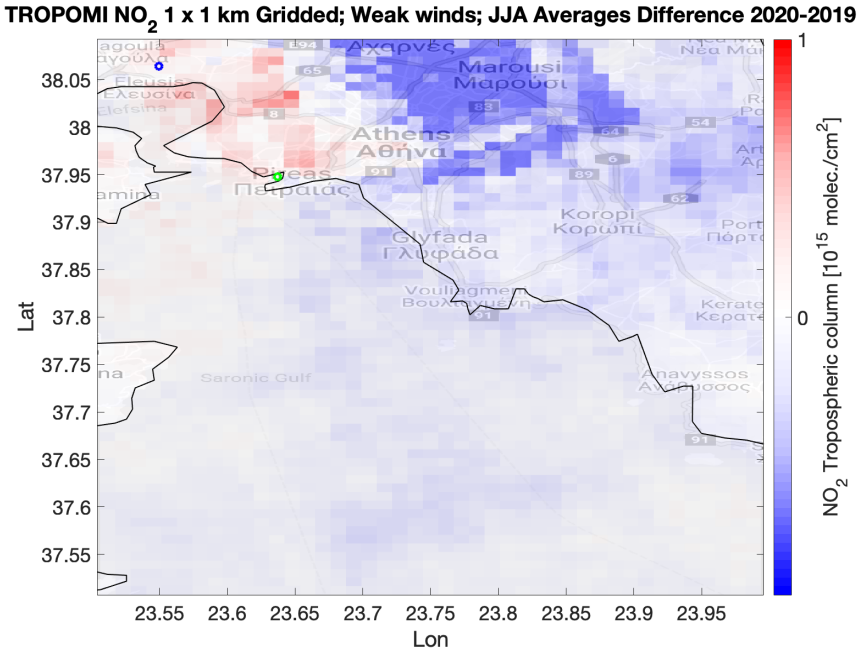

Figure 5.8: Difference between summer averages of 2020 and 2019 of TROPOMI tropospheric NO_2 column concentrations. Only days with weak wind are included (daily average wind velocity $< 5\text{ms}^{-1}$). Location of the Piraeus port is marked with a green circle, and the location of Eleusis airport with dark blue circle.

average NO_2 column concentration was actually larger compared to 2019. The fact that cargo ships were operating normally during spring 2020 could mean that at least some relevant shipping emission sources were contributing to the average concentration. The TROPOMI NO_2 concentrations were also averaged for the study areas A1, A2 and A3. In A1, average NO_2 concentration of spring 2020 was 31% smaller than the corresponding NO_2 concentration of spring 2019. Instead in A2, the spring 2020 average concentration was 10% larger than the 2019 average. In A3, the difference between spring averages of years 2020 and 2019 was just 4%, the 2020 average being slightly larger. This could also indicate that the shipping emissions over the sea were less affected by the restrictions compared to urban emission sources, as the differences in A2 and A3 were opposite compared to A1.

Figure 5.8 is similar to 5.7, but it shows the difference between averaged TROPOMI NO_2 of summer months (JJA) of 2020 and 2019. Here, the difference for the summer months is not as clear as in spring. In area A1, the difference between summer averages of 2019 and 2020 is minor. In A2, summer 2020 had 7% lower average than 2019, whereas in A3, summer 2020 had 14% lower average than 2019. As world trade experienced unexpected changes during year 2020, that could be the reason why the shipping emissions were slightly smaller than typical in summer 2020. Also, anthropogenic activities remained lower than typical, resulting in lower concentrations in urban areas. Therefore, there were smaller amount of urban emissions to be transported over the sea.

Next, the study areas A1, A2 and A3 are considered separately in more detail. Figure 5.9 shows time series of 14 day averages during spring of 2019 and 2020. Only observations that have weak wind conditions (wind velocity < 5 ms^{-1}) are included in the averages. Comparing the three time series, it can be seen that the difference between years 2020 and 2019 was the most significant in Central Athens (A1). Especially during March 2020, NO_2 concentrations are clearly lower compared to the corresponding averages of year 2019. There is a clear decrease in NO_2 concentrations after the end of February and the beginning of March in 2020. The concentrations decreased steadily during March 2020. This decrease in emissions can be explained as restrictions started halfway March. In April, the difference between 2019 and 2020 becomes smaller and in May, NO_2 concentration averages in 2020 seem to be back to the same level as the averages of 2019. Results of Ref. [34] showed that ground based measurement stations in Athens observed high NO_2 concentrations just after the opening of businesses. That increase in concentrations is seen in the time series for areas A1 and A2 in May 2020. In area A2, which represents Piraeus port area, the differences between the averages of years 2020 and 2019 are not that clear compared to A1. However, actually the relative differences between 2019 and 2020 are almost similar magnitude as in A2, expect for

the large decrease in concentrations during end of March and start of April, that was more clear in A1. The average concentrations in A2 are smaller compared A1 from the beginning, so as large decrease as in A1 is not expected in A2.

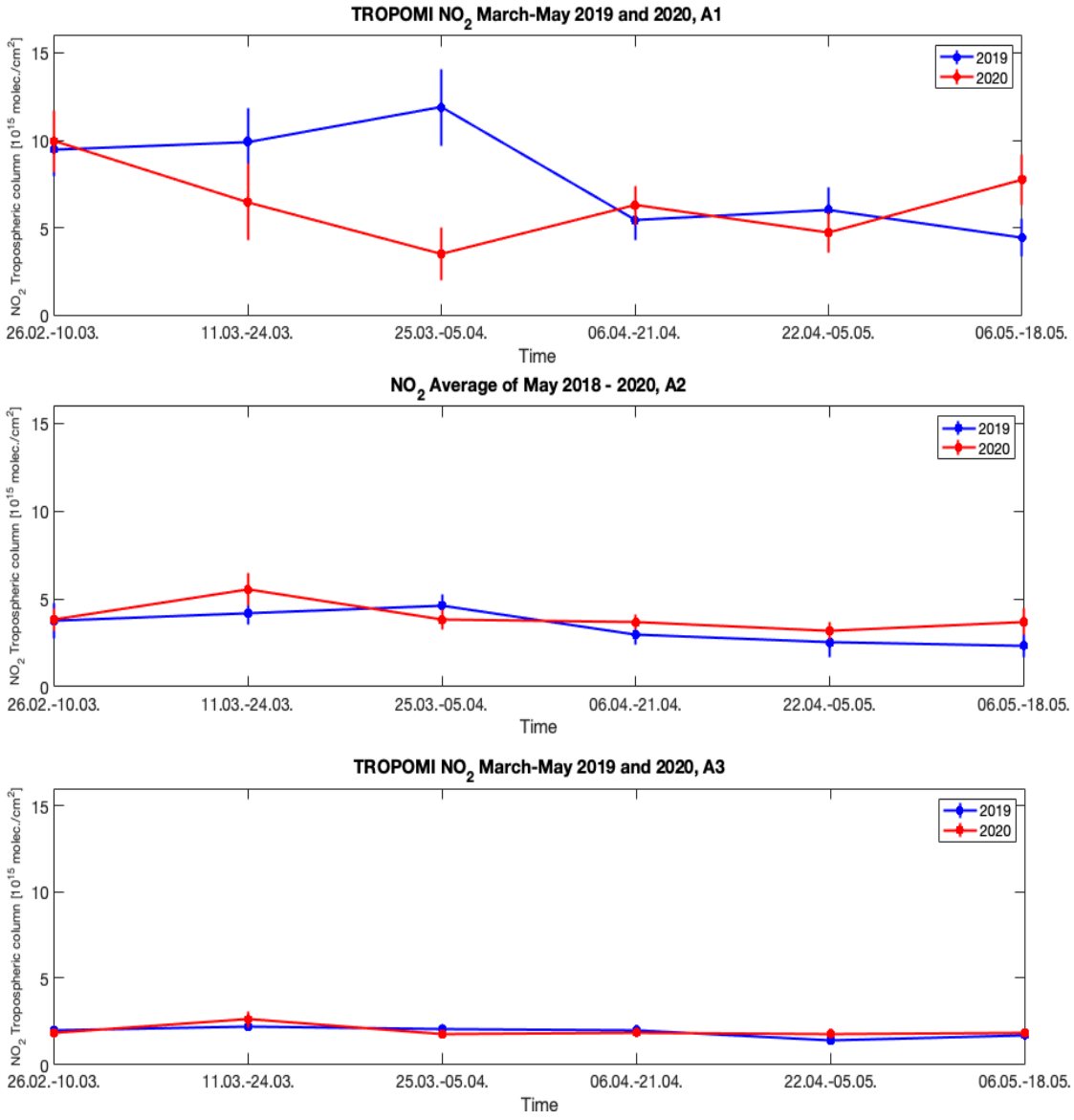

Figure 5.9: Time series of 14 day averages of TROPOMI NO_2 tropospheric column concentrations in i) Central Athens (A1) ii) Piraeus port (A2) and iii) shipping lane area close to Athens (A3). In Athens, the lockdowns started on 13 March 2020 and ended on 11 May 2020. Data is filtered according to the TROPOMI quality flag and a wind speed filter so that observations with wind speed 5ms^{-1} or stronger are removed.

For A3, there is no clear difference between averages of 2019 and 2020. Also relatively, the differences between 2019 and 2020 were smaller in A3 compared to A1 and A2. Overall, slightly higher NO_2 concentrations were observed in 2020 compared to 2019. Container terminals of Piraeus port operated normally during spring 2020, and the volume even increased in 2020 compared to 2019 [36]. That is why it is expected that the shipping emissions were produced normally.

It should be noted that the observed changes in NO_2 concentrations are not necessarily solely caused by changes in anthropogenic activities. Comparison of small temporal scale averages can be difficult, because the measuring conditions like meteorological variables and the viewing conditions vary. Also satellite observation sampling can be uneven, as the quality flag filtering is done for both years. To consider these points that could affect the interpretation of the results, an analysis on meteorological conditions of the considered measurement time periods is done for both years. Meteorological parameters that are observed here are daily averaged air temperatures, wind velocities and cloud radiance fractions (CRF). The temperature and wind data are from ground-based measurement station in Eleusis airport, and the CRF is a measurement variable of TROPOMI. Wind observations from the ground-based station are also supported by the gridded ERA5 reanalysis data that has been used in this thesis.

Figure 5.10 shows the time series of daily averaged air temperature observations from Elesius airport, for spring 2019 and 2020. Temperatures seem to be typical for spring for both years. Temperature observations do not indicate that there would have been unusual weather affecting the satellite observation quality.

Figure 5.11 shows daily averaged wind velocity measurements from Elesius airport, for years 2019 and 2020. In this case, wind is considered strong if the velocity is larger than 5 ms^{-1}. Both years have 7 days when the daily average wind velocity was strong. Based on this, the wind filtering effect was equal for both years. However, in 2019 the winds were stronger during March whereas in 2020 winds were stronger in April.

Figure 5.12 shows TROPOMI Level 2 cloud radiance fraction (CRF) averaged for area A1. CRF value indicates the fraction of the satellite pixel that is covered by clouds. If CRF value is larger that 0.5, TROPOMI quality flag defines that satellite retrieval cannot be made. On average, cloudiness affected satellite measurements of 2019 more, as 19 days are not approved by the quality flag. In reference, 2020 had 14 unqualified days. However, the difference is not that big it could fully explain the observed differences between 2019 and 2020 averages.

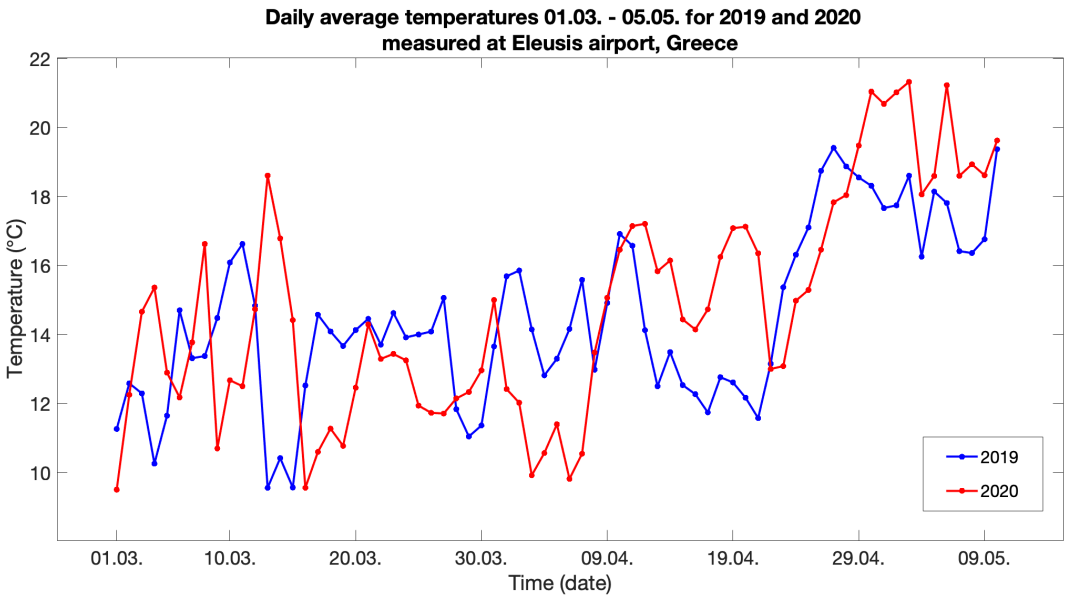

Figure 5.10: Daily averaged temperature measurements from Elesius airport, during 01. March - 09. May for 2019 and 2020. Data is free to download from www.rp5.ru.

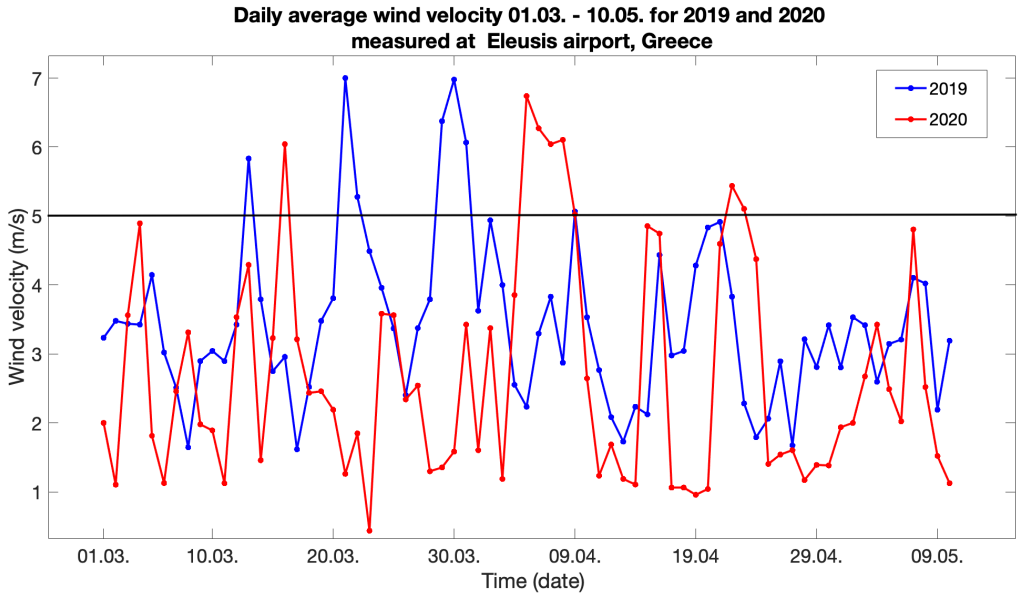

Figure 5.11: Daily averaged wind velocity measurements from Elesius airport, during 01. March - 09. May for 2019 and 2020. Data is free to download from www.rp5.ru. A limit is marked at 5ms^{-1} to characterize the limit used to classify strong and weak winds.

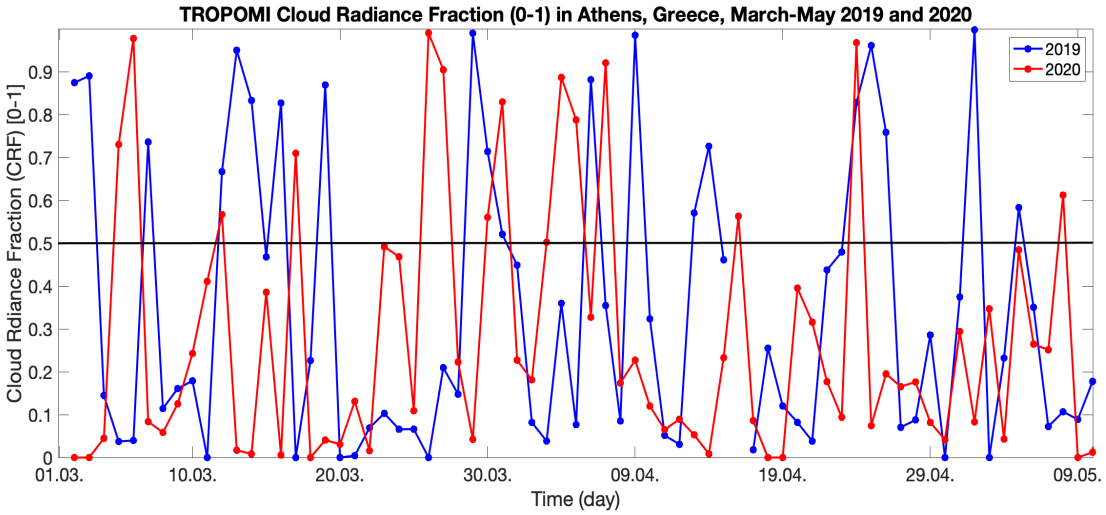

Figure 5.12: TROPOMI Cloud Radiance Fraction (CRF) averaged daily on area A1.

Overall, both years have only normal variations in temperatures, wind velocities and cloudiness. Based on that, it is assumed that the meteorological conditions did not affect the data quality that much it would have caused as large decline in concentrations as was observed. Also there was no situation where one year would have been significantly more affected by quality flag or wind filtering.

6. Conclusions and discussion

The objective of this thesis was to test the sensitivity of satellite measurements to characterize signatures of shipping emissions of NO_2 over the Eastern Mediterranean. This was done to discuss how satellite measurements could be used as a tool in shipping emission monitoring. An overview was done for the whole area, and a more detailed study was executed close to Athens and port Piraeus. As TROPOMI measurements estimate the total amount of NO_2 molecules in a tropospheric column, additional information was required to investigate the signal of shipping emissions. In this thesis, the analysis methods included averaging data on smaller study areas and comparing TROPOMI tropospheric NO_2 measurements to model products of AIS messages and exhaust shipping emissions of NO_x. These two model datasets were provided by Ship Traffic Emission Assessment Model (STEAM).

The results showed that over the whole Eastern Mediterranean area, the busiest shipping lanes and the largest ports could be detected as elevated TROPOMI NO_2 concentrations. It was assessed that close to the coast, also wind conditions affected how easily the shipping emissions could be observed. If the dominant wind direction was from the continent towards the sea, then the satellite observations would show more clearly elevated concentrations over areas with busy ship traffic. Over the sea, elevated NO_2 concentrations coincided with STEAM NO_x emissions quite well. TROPOMI observations showed line-shaped elevated concentrations over a busy shipping lane, where also STEAM results showed NO_x emissions. Data comparison over the shipping lane area revealed that it is difficult to detect the signal of shipping emissions over areas where the monthly summed shipping NO_x emission amount was small, approximately 100 tonnes or smaller. On the contrary, the sea areas that had monthly summed shipping emission amount over 1000 tonnes did not correspond to as high level of TROPOMI NO_2 as would have been expected. When investigating the TROPOMI measurements in single grid cell, it showed that the elevated NO_2 observations are minority compared to background concentrations. That means that the shipping emission signal was averaged out. The comparison of grid cells could possibly show a better relation if the grid cells were averaged into a resolution that is more close to the original resolution of TROPOMI.

TROPOMI and STEAM comparison was also done with finer resolution in port Piraeus and over the sea south from the port. Monthly average concentrations of the areas showed that the area over the sea (A3) should be less affected by urban emissions than the port area, despite knowing that the dominant wind is from the port towards the sea. The result showed that over the sea, monthly summed shipping emissions of NO_x and monthly medians of TROPOMI NO_2 tropospheric columns had a nearly statistically significant relationship. It means that within that distance (35 km from the coast), satellite measurements had a signal of shipping emissions, and therefore offer an tool for shipping emission monitoring. When the same analysis was applied for the sea area attached to the port Piraeus, there was no relation between TROPOMI and STEAM. It indicates that the port area is influenced by other emission sources, and therefore the shipping emission signal is not easily detected. Monthly summed AIS messages did not show correlation with monthly medians of TROPOMI NO_2 concentrations, indicating that gridded AIS messages was not suitable product for this kind of analysis. More careful filtering of AIS data could be done to find a relation with satellite observations. Shipping emission signal can be difficult to distinguish when urban emissions are having a dominant role also close to the coast. Additional research on different area could also confirm that the AIS messages are overall bad indicator for shipping activity in this kind of comparison.

Lastly, a separate study was executed to see how air quality of the different study areas was affected by COVID-19 pandemic restrictions, and how TROPOMI measurements would detect the possible rapid changes of NO_2 concentrations in spring 2020. In the city centre of Athens, spring 2020 average was 31% smaller compared to 2019 average. The magnitude of the difference between years 2019 and 2020 was at the same scale as found in other studies [35]. However, spring month averages of the Piraeus port area and the shipping lane area showed small to non-existent decrease in 2020. It suggests that the pandemic had only minor effect on shipping emissions during spring 2020. Meteorological conditions did not show anything that would fully explain the differences between 2019 and 2020 average concentrations.

The results of this thesis showed that finding shipping emission signals from satellite observations is not a straightforward task. The emission signals seem to still depend closely on the observation location and the wind conditions. More careful filtering of the data could improve the results close to the port area. The methods of this thesis could also be applied to a sea area that is not close to as densely populated city as Athens. Nevertheless, the results of this thesis already indicated a possibility that satellite observations could be used as a tool for shipping emission monitoring over the open sea areas, where the need for shipping emission monitoring techniques is more urgent, as ground-based measurements are non-existent.

Bibliography

[1] World Shipping Council. About the industry: global trade. https://www.worldshipping.org/about-the-industry/global-trade. Last Access: 12 April 2021.

[2] International Maritime Organization. Marine environment. https://www.imo.org/en/OurWork/Environment/Pages/Default.aspx. Last Access: 20 May 2021.

[3] J. J. Corbett and H. W. Koehler. Updated emissions from ocean shipping. *J. Geophys. Res.*, 108, 2003.

[4] M. Sofiev, J.J. Winebrake, L. Johansson, W. Edward, W. Carr, M. Prank, J. Soares, J. Vira, R. Kouznetsov, Jalkanen J.-P., and J.J. Corbett. Cleaner fuels for ships provide public health benefits with climate tradeoffs. *Nat. Commun.*, 9(406), 2018.

[5] T.-H. Joung, S.-G. Kang, J.-K. Lee, and J. Ahn. The IMO initial strategy for reducing greenhouse gas (GHG) emissions, and its follow-up actions towards 2050. *Journal of International Maritime Safety, Environmental Affairs, and Shipping*, 4(1):1–7, 2020.

[6] European Environment Agency. The impact of international shipping on European air quality and climate forcing. *EEA Technical report. Luxembourg: Publications Office of the European Union*, 2013.

[7] International Maritime Organization. Prevention of air pollution from ships and NOx technical code. *MARPOL ANNEX VI convention 73/78, London*, 1998.

[8] International Maritime Organization. Nitrogen Oxides (NOx). *IMO MARPOL ANNEX VI regulation 13*, 1997.

[9] International Maritime Organization. Sulphur oxides (SOx) and Particulate Matter (PM). *IMO MARPOL ANNEX VI regulation 14*, 1997.

[10] The SCIPPER Project. https://www.scipper-project.eu, 2020. Last Access: 29 April 2021.

[11] J.H.G.M. van Geffen, H. J. Eskes, K. F. Boersma, J. D. Maasakkers, and J. P. Veefkind. TROPOMI ATBD of the total and tropospheric NO2 data products.Royal Netherlands Meteorological Institute (KNMI). *S5P-KNMI-L2-0005-RP,CI-7430-ATBD, version 1.4.0*, 2019.

[12] I. Ialongo, H. Virta, H. Eskes, J. Hovila, and J. Douros. Comparison of TROPOMI/Sentinel-5 Precursor NO2 observations with ground-based measurements in Helsinki. *Atmos. Meas. Tech.*, 13:205–218, 2020.

[13] J.-P. Jalkanen, L. Johansson, J. Kukkonen, A. Brink, J. Kalli, and T. Stipa. Extension of an assessment model of ship traffic exhaust emissions for particulate matter and carbon monoxide. *Atmospheric Chemistry and Physics Discussions*, 11:22129–22172, 08 2012.

[14] M. Bauwens, S. Compernolle, T. Stavrakou, J.F. Müller, J. van Gent, H. Eskes, and et al. Impact of coronavirus outbreak on NO2 pollution assessed using TROPOMI and OMI observations. *Geophysical Research Letters*, 47, 2020.

[15] D. J. Jacob. *Introduction to Atmospheric Chemistry.* Princeton, N.J: Princeton University Press, 1999.

[16] H. Karttunen, J. Koistinen, E. Saltikoff, and O. Manner. *Ilmakehä, sää ja ilmasto (in Finnish).* Ursan tieteellisiä julkaisuja 107, 2008.

[17] U. Platt and J. Stutz. *Differential Optical Absorption Spectroscopy: Principles And Applications.* Physics of Earth and Space Environments, 2008.

[18] J. Calvert, A. Mellouki, J. Orlando, M. Pilling, and T. Wallington. *Mechanisms of Atmospheric Oxidation of the Oxygenates.* Oxford University Press, 2011.

[19] R. G. Prinn. *Ozone, hydroxyl radical and oxidative capacity. The Atmosphere (ed. R.F. Keeling)*, volume 4, chapter 1, pages 1–19. Treatise on Geochemistry Elsevier-Pergamon, Oxford, 2003.

[20] C. H. Song, G. Chen, S. R. Hanna, J. Crawford, and D. D. Davis. Dispersion and chemical evolution of ship plumes in the marine boundary layer: Investigation of O3/NOy/HOx chemistry. *J. Geophys. Res.*, 108(D4), 4143, 2003.

[21] D. Vallero. *Fundamentals of Air Pollution, Fourth edition.* Academic Press, 2008.

[22] IPCC. *Climate Change 2007: The Physical Scince basis. Contribution of Working group I to the Fourth Assesment Report of the Intergovernmental Panel on Climate Change [Solomon, S., D. Qin, M. Manning, Z. Chen, M. Marquis, K.B.*

Averyt, M. Tignor and H.L. Miller], chapter 7: Coupling Between Changes in the Climate System and Biochemistry. Cambridge University Press, Cambridge, United Kingdom and New York NY, USA, 2007.

[23] S. Beirle, U. Platt, R. von Glasow, M. Wenig, and T. Wagner. Estimate of nitrogen oxide emissions from shipping by satellite remote sensing. *Geophysical Research Letters*, 31, L18102, 2004.

[24] T. Stavrakou, J.-F. Müller, K. F. Boersma, R. J. van der A, J. Kurokawa, T. Ohara, and Q Zhang. Key chemical NOx sink uncertainties and how they influence top-down emissions of nitrogen oxides. *Atmos. Chem. Phys.*, 13:9057–9082, 2013.

[25] European Environment Agency. Air quality in Europe - 2020 report. *Luxembourg: Publications Office of the European Union*, 2020.

[26] European Environment Agency EEA. European Union emission inventory report 1990-2011 under the UNECE Convention on Long-range Transboundary Air Pollution (LRTAP). *EEA Technical report. Luxembourg: Publications Office of the European Union*, 10, 2013.

[27] J. Corbett, J. Winebrake, E. Green, P. Kasibhatla, V. Eyring, and A. Lauer. Mortality from ship emissions: A global assessment. *Environmental science and technology*, 41:8512–8, 01 2007.

[28] United States Environmental Protection Agency. Effects of acid rain. https://www.epa.gov/acidrain/effects-acid-rain. Last Access: 20 April 2021.

[29] A. Colette, C. Granier, Ø. Hodnebrog, H. Jakobs, A. Maurizi, A. Nyiri, B. Bessagnet, A. D'Angiola, M. D'Isidoro, M. Gauss, F. Meleux, M. Memmesheimer, A. Mieville, L. Rouïl, F. Russo, S. Solberg, F. Stordal, and F. Tampieri. Air quality trends in Europe over the past decade: a first multi-model assessment. *Atmospheric Chemistry and Physics*, 11(22):11657–11678, 2011.

[30] International Maritime Organization. MEPC 75/7/15: reduction of GHG emissions from ships: Fourth IMO GHG study 2020 - final report. *IMO Arctic Summit, July 29*, 2020.

[31] J. Cofala, M. Amann, C. Heyes, F. Wagner, Z. Klimont, M. Posch, W. Schoepp, L. Tarasson, J. Jonson, C. Whall, and A. Stavrakaki. *Analysis of Policy Measures to Reduce Ship Emissions in the Context of the Revision of the National Emissions Ceilings Directive*. International Institute for Applied Systems Analysis (IIASA), 01 2007.

[32] World Health Organization R&D Blue Print. COVID-19 public health emergency of international concern (PHEIC). *Global research and innovation forum*, 02 2020.

[33] World Health Organization. WHO coronavirus (COVID-19) dashboard - Greece. https://covid19.who.int/region/euro/country/gr. Last Access: 18 May 2021.

[34] C. Varotsos, J. Christodoulakis, G.A. Kouremadas, and E.-F. Fotaki. The signature of the coronavirus lockdown in air pollution in Greece. *Water, Air & Soil Pollut*, 232(119), 2021.

[35] M.-E. Koukouli, I. Skoulidou, A. Karavias, I. Parcharidis, D. Balis, A. Manders, A. Segers, H. Eskes, and J. van Geffen. Sudden changes in nitrogen dioxide emissions over Greece due to lockdown after the outbreak of COVID-19. *Atmos. Chem. Phys.*, 21:1759–1774, 2021.

[36] Piraeus port authority S.A. Annual financial report: For the year ended December 31, 2020. *Intestor relations/Annual reports*, 2021.

[37] World Shipping Council. About the industry: TOP 50 WORLD CONTAINER PORTS. https://www.worldshipping.org/about-the-industry/global-trade/top-50-world-container-ports. Last Access: 20. April 2021.

[38] Hellenic Shipping News. Greece's Piraeus port posts positive financial results for 2019. *Hellenic Shipping News Worldwide*, 07 2020.

[39] K. Bogumil, J. Orphal, T. Homann, S. Voigt, P. Spietz, O.C. Fleischmann, A. Vogel, M. Hartmann, H. Kromminga, H. Bovensmann, J. Frerick, and J.P. Burrows. Measurements of molecular absorption spectra with the SCIAMACHY pre-flight model: instrument characterization and reference data for atmospheric remote-sensing in the 230-2380 nm region. *Journal of Photochemistry and Photobiology A: Chemistry*, 157(2):167–184, 2003. Atmospheric Photochemistry.

[40] K. F. Boersma, H. J. Eskes, J. P. Veefkind, E. J. Brinksma, R. J. van der A, and et al. Near-real time retrieval of tropospheric NO2 from OMI. *Atmospheric Chemistry and Physics*, 7:2103–2118, 2007.

[41] A. Lorente, K. Folkert Boersma, H. Yu, S. Dörner, A. Hilboll, A. Richter, M. Liu, L. N. Lamsal, M. Barkley, I. De Smedt, M. Van Roozendael, Y. Wang, T. Wagner, S. Beirle, J.-T. Lin, N. Krotkov, P. Stammes, P. Wang, H. J. Eskes, and M. Krol. Structural uncertainty in air mass factor calculation for NO_2 and HCHO satellite retrievals. *Atmospheric Measurement Techniques*, 10(3):759–782, 2017.

[42] T. Verhoelst, S. Compernolle, G. Pinardi, J.-C. Lambert, H. J. Eskes, K.-U. Eichmann, A. M. Fjæraa, J. Granville, S. Niemeijer, A. Cede, M. Tiefengraber, F. Hendrick, A. Pazmiño, A. Bais, A. Bazureau, K. F. Boersma, K. Bognar, A. Dehn, S. Donner, A. Elokhov, M. Gebetsberger, F. Goutail, M. Grutter de la Mora, A. Gruzdev, M. Gratsea, G. H. Hansen, H. Irie, N. Jepsen, Y. Kanaya, D. Karagkiozidis, R. Kivi, K. Kreher, P. F. Levelt, C. Liu, M. Müller, M. Navarro Comas, A. J. M. Piters, J.-P. Pommereau, T. Portafaix, C. Prados-Roman, O. Puentedura, R. Querel, J. Remmers, A. Richter, J. Rimmer, C. Rivera Cárdenas, L. Saavedra de Miguel, V. P. Sinyakov, W. Stremme, K. Strong, M. Van Roozendael, J. P. Veefkind, T. Wagner, F. Wittrock, M. Yela González, and C. Zehner. Ground-based validation of the Copernicus Sentinel-5P TROPOMI NO_2 measurements with the NDACC ZSL-DOAS, MAX-DOAS and Pandonia global networks. *Atmospheric Measurement Techniques*, 14(1):481–510, 2021.

[43] J.P. Burrows, M. Weber, M. Buchwitz, V. Rozanov, A. Ladstätter-Weishenmayer, A. Richter, R. DeBeek, R. Hoogen, K. Bramstedt, K.-U. Eichmann, M. Eisinger, and D. Perner. The global ozone monitoring experiment (GOME): Mission Concept and First Scientific Results. *Journal of the Atmospheric Sciences*, 56(2):151–175, 1999.

[44] H. Bovensmann, J. Burrows, M. Buchwitz, J. Frerick, S. Noel, V. Rozanov, K. Chance, and A. Goede. SCIAMACHY: Mission objectives and measurement modes. *J. Atmos. Sci.*, 56:127–150, 01 1999.

[45] A. Richter, V. Eyring, . P. Burrows, H. Bovensmann, A. Lauer, B. Sierk, and P. J. Crutzen. Satellite measurements of NO2 from international shipping emissions. *Geophysical Research Letters*, 31(23), 2004.

[46] P. F. Levelt, van den G. H. J. Oord, M. R. Dobber, A. Mälkki, H. J. Visser, J. de Vries, ..., and H Saari. The ozone monitoring instrument. *IEEE Transactions on Geoscience and Remote Sensing*, 44(5):1093–1101, 2006.

[47] I. Ialongo, J. Hakkarainen, N. Hyttinen, J.-P. Jalkanen, L. Johansson, K. F. Boersma, N. Krotkov, and J. Tamminen. Characterization of OMI tropospheric NO2 over the Baltic Sea region. *Atmos. Chem. Phys.*, 14:7795–7805, 2014.

[48] G. C. M. Vinken, K. F. Boersma, A. van Donkelaar, and L. Zhang. Constraints on ship NOx emissions in europe using GEOS-Chem and OMI satellite NO2 observations. *Atmos. Chem. Phys.*, 14:1353–1369, 2014.

[49] M. Schaap, R. Kranenburg, L. Curier, M. Jozwicka, E. Dammers, and R. Timmermans. Assessing the sensitivity of the OMI-NO2 product to emission changes across Europe. *Remote Sens.*, 5:4187–4208, 2013.

[50] J.P. Veefkind, I. Aben, K. McMullan, H. Förster, J. de Vries, G. Otter, J. Claas, H.J. Eskes, J.F. de Haan, Q. Kleipool, M. van Weele, O. Hasekamp, R. Hoogeveen, J. Landgraf, R. Snel, P. Tol, P. Ingmann, R. Voors, B. Kruizinga, R. Vink, H. Visser, and P.F. Levelt. TROPOMI on the ESA Sentinel-5 Precursor: A GMES mission for global observations of the atmospheric composition for climate, air quality and ozone layer applications. *Remote Sensing of Environment*, 120:70–83, 2012. The Sentinel Missions - New Opportunities for Science.

[51] KNMI The Royal Netherlands Meteorological Institute. Algorithm theoretical basis document for the TROPOMI L01b data processor. *Tech. Rep. S5P-KNMI-L01B-0009-SD, Koninklijk Nederlands Meteorologisch Instituut (KNMI), CI-6480-ATBD*, issue 8.0.0, 2017.

[52] A.-M. Sundström, H. Virta, I. Ialongo, and J. Tamminen. Satelliittihavaintojen hyödyntäminen ilmanlaadun seurannassa (in Finnish). *Raportteja*, 1:2020, 2020. Ilmatieteenlaitos.

[53] A. K. Georgoulias, K. F. Boersma, J. van Vliet, X. Zhang, R. van der A, P. Zanis, and J. de Laat. Detection of NO2 pollution plumes from individual ships with the TROPOMI/S5P satellite sensor. *Environmental Research Letters*, 2020.

[54] S. Beirle, K.F. Boersma, U. Platt, M.G. Lawrence, and T. Wagner. Megacity emissions and lifetimes of nitrogen oxides probed from space. *Science*, 333(6050):1737–9, 2011.

[55] H. Hersbach. The ERA5 atmospheric reanalysis. *American Geophysical Union, Fall Meeting 2016, abstract NG33D-01*, 12 2016.

[56] M.A. Russo, J. Leitao, C. Gama, J. Ferreira, and A. Monteiro. Shipping emissions over Europe: A state-of-the-art and comparative analysis. *Atmospheric Environment*, 177:187–194, 2018.

[57] International Maritime Organization. Safety of life at sea (SOLAS) agreement. *Chapter V - Safety of navigation*, 2000. Amendments.

[58] J.-P. Jalkanen, A. Brink, J. Kalli, H. Pettersson, J. Kukkonen, and T. Stipa. A modelling system for the exhaust emissions of marine traffic and its application in the Baltic Sea area. *Atmos. Chem. Phys.*, 9:9209–9223, 2009.

[59] J.-P. Jalkanen, L. Johansson, and J. Kukkonen. A comprehensive inventory of ship traffic exhaust emissions in the European sea areas in 2011. *Atmospheric Chemistry and Physics*, 16, 01 2016.

[60] K. Sun, L. Zhu, K. Cady-Pereira, C. Chan Miller, K. Chance, L. Clarisse, P.-F. Coheur, G. González Abad, G. Huang, X. Liu, M. Van Damme, K. Yang, and M. Zondlo. A physics-based approach to oversample multi-satellite, multi-species observations to a common grid. *Atmospheric Measurement Techniques*, 11(12):6679–6701, 2018.

[61] Finnish Meteorological Institute. Tuulet ja myrskyt: Tuulen suunta (in Finnish). https://www.ilmatieteenlaitos.fi/tuulet. Last Access: 10 May 2021.

[62] MathWorks Documentation. Linear regression: Residuals and goodness of fit. https://se.mathworks.com/help/matlab/data_analysis/linear-regression.html#f1-15010. Last Access: 20 May 2021.

[63] M. Krzywinski and N. Altman. Significance, p values and t-tests. *Nat Methods*, 10:1041–1042, 2013.

[64] M.S. Thiese, B. Ronna, and U. Ott. P value interpretations and considerations. *J Thorac Dis.*, 8(9):928–931, 2016.

[65] H2020 EMERGE. Evaluation, control and Mitigation of the EnviRonmental impacts of shippinG Emissions. https://emerge-h2020.eu/. Last Access: 31 March 2021.

[66] E. Tzannatos. Ship emissions and their externalities for the port of Piraeus - Greece. *Atmospheric Environment*, 44:400–407, 01 2010.

[67] Z. Bar-Yehuda. zoharby/plot_google_map. https://github.com/zoharby/plot{_}google{_}map. GitHub. Retrieved 23 April 2021.

[68] C. Deniz and Y. Durmusoglu. Estimating shipping emissions in the region of the Sea of Marmara, Turkey. *The Science of the total environment*, 390:255–61, 03 2008.

[69] C. A. Greene and et al. The Climate Data Toolbox for MATLAB. *Geochemistry, Geophysics, Geosystems, American Geophysical Union (AGU)*, 07 2019.

[70] D. Roberts-Semple, F. Song, and Y. Gao. Seasonal characteristics of ambient nitrogen oxides and ground-level ozone in metropolitan northeastern New Jersey. *Atmospheric Pollution Research*, 3(2):247–257, 2012.

[71] European Environment Agency. Air pollution in Athens: existing status and abatement practices. https://www.eea.europa.eu/publications/2599XXX/page018.html. Last Access: 10 May 2021.

[72] A. Mavrakis, A. Kapsali, I.X. Tsiros, and Pantavou K. Air quality and meteorological patterns of an early spring heatwave event in an industrialized area of Attica, Greece. *Euro-Mediterranean Journal for Environmental Integration*, 6(25), 2021.